





Article

Intelligent Assessment of Pavement Condition Indices Using Artificial Neural Networks

Sami Abdullah Osman ¹, Meshal Almoshaogeh ^{2,*}, Arshad Jamal ^{1,*}, Fawaz Alharbi ²,
Abdulhamid Al Mojil ¹ and Muhammad Abubakar Dalhat ¹

¹ Transportation and Traffic Engineering Department, College of Engineering, Imam Abdulrahman Bin Faisal University, P.O. Box 1982, Dammam 31451, Saudi Arabia

² Department of Civil Engineering, College of Engineering, Qassim University, Buraidah 51452, Saudi Arabia

* Correspondence: m.moshaogeh@qu.edu.sa (M.A.); ajjamal@iau.edu.sa (A.J.)

Abstract: The traditional manual approach of pavement condition evaluation is being replaced by more sophisticated automated vehicle systems. Although these automated systems have eased and hastened pavement management processes, research is ongoing to further improve their performances. An average state road agency handles thousands of kilometers of the road network, most of which have multiple lanes. Yet, for practical reasons, these automated systems are designed to evaluate road networks one lane at a time. This requires time, energy, and possibly more equipment and manpower. Multiple Linear Regression (MLR) analysis and Artificial Neural Network (ANN) were employed to examine the feasibility of modeling and predicting pavement distresses of multiple lanes as functions of pavement distresses of a single adjacent lane. The successful implementation of this technique has the potential to cut the energy and time requirement at the condition evaluation stage by at least half, for a uniform multi-lane highway. Results showed promising model performances that indicate the possibility of evaluating a multi-lane highway pavement condition (PC) by single lane inspection. Traffic direction parameters, location, and lane matching parameters contributed significantly to the performance of the ANN PC prediction models.

Keywords: pavement condition; degradation; prediction; artificial intelligence; artificial neural network; regression analysis; pavement evaluation; Saudi Arabia



Citation: Osman, S.A.; Almoshaogeh, M.; Jamal, A.; Alharbi, F.; Al Mojil, A.; Dalhat, M.A. Intelligent Assessment of Pavement Condition Indices Using Artificial Neural Networks.

Sustainability **2023**, *15*, 561. <https://doi.org/10.3390/su15010561>

Academic Editors: Luigi Pariota and Francesco Abbondati

Received: 28 October 2022

Revised: 16 November 2022

Accepted: 29 November 2022

Published: 28 December 2022



Copyright: © 2022 by the authors. Licensee MDPI, Basel, Switzerland. This article is an open access article distributed under the terms and conditions of the Creative Commons Attribution (CC BY) license (<https://creativecommons.org/licenses/by/4.0/>).

1. Introduction

Artificial intelligence (AI) is an emerging area of computer science that uses different types of machines and sensors to mimic intelligent human behavior. John McCarthy first introduced AI in 1956 [1]; however, lack of technological innovations by the time limited its applications. In the following decade (between 1960 to 1970) researchers explored AI through artificial neural networks (ANNs) and Knowledge-based systems (KBS) [1]. ANNs are systems of neurons connected in various layers and inspired by the human brain to solve various complex real-life tasks. On the other hand, KBS systems are computers that offer guidance based on pre-established rules based on the information fed to them by humans. Application of the latest Machine Learning (ML) and Deep Learning (DL) based technologies have revolutionized AI. ML and DL have found various applications in diverse fields such as face recognition and tracking [2], visual tracking [3,4], vision and language navigation [5–7], and image and video editing [8–10]. In recent years, application of such soft computing methodologies has received widespread applications for various civil and transportation engineering-related problems, including road safety [11–14], mode choice modeling [15], energy demand modeling for electric vehicles [16–18], and traffic sign detection and recognition [19,20]. Similarly, applications of these predictive modeling approaches are reshaping the field of pavement evaluation and management.

Quality road networks are key to the safe movement of people, goods, and transfer of services. These are transportation aspects that facilitate the social and economic development of all nations. However, quality roads can only be maintained through an efficient pavement management system. Due to the significance of establishing and maintaining good road network, all responsible governments and road management agencies around the globe continue to invest and adopt modern tools in managing the pavement conditions of their highway networks. Artificial intelligence techniques such as Expert Systems, ANN, Genetic Algorithms, and Hybrid Systems have found a wide range of applications in three key stages of pavement management systems [21–23]. These stages include pavement distresses or deterioration diagnosis and modeling [24–27], identification and selection of maintenance action [28], and systematic prioritization and optimization of pavement maintenance [21,29]. The pavement distress identification and modeling stages formed the basis and building blocks to achieving the second and third most important management stages. The use of conventional regression analysis in modeling Pavement Conditions (PC) as functions of distresses has often resulted in poor and inaccurate relationships [22]. This is due to the random nature of the PC data that contain irregular data points which naïve statistical analysis would regard as outliers. This is evident from a recent study that gives a statistical insight into whether the International Roughness Index (IRI) should be considered as an alternative distress and a ride quality index [30]. Although most of the pavement's distresses showed a statistically significant relationship with the IRI, only about 30% of the IRI data can be described by the developed models. In another study, IRI was successfully modeled as a function of traffic, time, and pavement structural inputs using higher-order polynomials [31,32]. However, the ANN modeling of the same data showed better performance by far. MLR and Neuro-Fuzzy algorithm were employed in modeling the pavement present serviceability index (PSI) as a function of traffic loading, rutting, and non-destructive deflection testing structural performance parameters [33]. Even though the Neuro-Fuzzy models showed slightly better prediction performance, the MLR models were also able to satisfactorily predict the PSI. However, the findings of an earlier study showed the inadequacy of MLR in modeling the IRI as a function of material and construction variables [25]. Back-propagated NN models were alternatively developed, revealing insightful and accurate relationships. In some cases where both MLR and Artificial Intelligence (AI) models performed satisfactorily, MLR models are preferred due to their simplicity [34]. Cluster-wise MLR models were also successfully employed to capture the heterogeneity in pavement deterioration [35]. In summary, regression analysis is often not adequate for modeling pavement performances, but it can sometimes yield the desired results. This is why several road agencies still use pavement management frameworks that utilize regression-based prediction models [36].

ANN self-organizing maps was earlier successfully used to develop a method for pavement distress grouping that will enable and ease pavement performance modeling [37]. The study illustrates how roughness was dependent on and can be modeled as a function of the grouped variables. However, the observed models' structures were not tested on numerical data to show their statistical performances. A method for selecting optimal major maintenance action based on ANN accident and sideway force predicting models was proposed [28]. Genetic algorithm (GA) was used to generate and select the optimal type of maintenance from the ANN model outputs. Levenberg–Marquardt algorithm was used to train and test the various two-layer neural networks (NN) without validation. Minimal error, correlation of 0.888, and 0.853 between the target and predicted output for training and testing were observed, respectively. ANN and GA were also employed to develop predictive model for PC Index (PCI) as alternative to the conventional chart-to-chart procedure [24]. The model was based on eight types of field-obtained pavement distresses and their severity levels from more than 12,000 pavement sections. The ANN model was more accurate with less than 1.00 Root Mean Square Error (RMSE), and 0.99 correlation with the target PCI. Hybrid feed-forward NN-GA algorithm was used to develop predictive models for airfield pavement deflection based on non-destructive testing moduli data

base [26]. The NN-GA predicted deflections showed a correlation above 0.99 with the measured deflections for both the pavement and sub-grade layers. A two-layer recurrent NN along with decision tree support vector classifier was used to model pavement PSI as a function of material and structural properties, traffic and maintenance history, and time [38]. Data pre-processing of IRI into clusters using k-mean and fuzzy c-mean was shown improve ANN model performance significantly [39]. The IRI model was a function of traffic and pavement structural variables.

In recent years, few studies have investigated the applicability of AI-based ML and DL frameworks for pavement condition evaluation and assessment. For example, Majidifard et al. employed a DL Yolo algorithm for automated pavement distress detection using a dataset containing 7237 Google street images [40]. Pavement condition was classified according to nine different distress classes. The authors were able to develop various pavement condition indices using the proposed algorithm, which can minimize human dependence for pavement inspection. Roberts et al. proposed a low-cost DL prediction methodology for pavement health condition monitoring [41]. The methodology was applied to a road network in Sicily, Italy to identify the hotspot locations of different pavement distress types and their severities which are in need of repair and rehabilitation. In another study, the researchers proposed an efficient pavement damage prediction model based on a thermal-*RGB* fusion [42]. The model achieved a fused image detection accuracy of 98%. Marcelino et al. utilized the International Roughness Index (IRI) for developing a Random Forest (RF)-based pavement performance prediction model in Pavement Management System (PMS) [43]. In addition to IRI data, other input data for the model were traffic, structural, and climate data. Sensitivity analysis showed that proposed RF model results were sensitive to previous IRI values. In their study, Inkoom et al. presented the application of ANNs and recursive partitioning frameworks for predicting the cracking rate in pavements [44]. Explanatory variables such as the roadway functional class, average daily traffic (considering truck factor), pavement condition time series data, and asphalt thickness were used for the model formulation. The recursive partitioning technique yielded promising results in terms of predictive accuracies 90.89–0.91), high ROC for the selected decision tree (DT) models, and efficient cost complexity. A recent study by Sholevar et al. a detailed literature review of various state-of-the-art ML techniques for pavement condition evaluation [45]. The review also highlighted the current challenges and prospects for future research in the domain of AI and ML for pavement distress identification and gradation of corresponding severities.

Based on the above literature review, although preferred due to their simplicity, the conventional modeling techniques such as regression analysis do not usually offer reliable prediction model for PC. In addition, these previous studies were mainly predicting individual PC such as IRI, PSI, and rutting, as function of material and traffic variables. In this study, ten PCI were considered for inter-lane PC prediction for efficient pavement management.

Problem Statement and Objective

More sophisticated automated vehicle systems are replacing the traditional manual approach of pavement condition evaluation. This was possible through continuous research on the application of AI techniques for pavement evaluation [45–47]. Such kind of smart pavement evaluation systems incorporate image processing and sensors [48–51], and many now exist commercially or as prototypes. Although these automated systems have eased and hastened pavement management processes, several pieces of research are ongoing to further improve their performances. An average state road agency handles thousands of kilometers of the road network, most of which have multiple lanes. Yet for practical reasons, these automated systems are designed to evaluate road networks one lane at a time. This means for a six-lane divided highway, the pavement inspection vehicle has to travel six times the distance of that road to fully cover the pavement sections. Time, energy, and data storages are costly, hence the question of whether this lane-by-lane practice will

be sustained for long arise. These automated pavement distress evaluation technologies are also not cheap. The question of whether this practice can be avoided by eliminating the need for full road coverage is evaluated in this study. Pavements are designed to last up to 20 years and even longer in some cases. If PC predictive models for adjacent lanes can be developed from single lanes for individual roads within such design lives of that road network, the task and efficiency of PC monitoring, evaluation, and maintenance could be further simplified and improved, respectively. Fundamental mathematical model for this problem does not exist, and based on the existing literature, no empirical mathematical model was previously reported or adopted to address this problem.

The objective of this study is to employ MLR analysis and ANN modeling to examine the feasibility of modeling and predicting the pavement distresses of multiple lanes as function of pavement distress of a single adjacent lane. The inter-lane PC indices modeling can also go a long way in facilitating more accurate forecasting models for estimating the future consequences of pavement maintenance actions.

2. Data and Methodology

Road condition indices of a two-way six-lane flexible highway were employed for this study. The pavement condition (PC) data were obtained from the Transport Ministry of Saudi Arabia. The data were captured by a state-of-the-art automated pavement evaluation vehicle (ARRB). The automated pavement evaluation system output includes six different PC indices for a given pavement section. Each lane in this study consists of 568 data sets of the various PC indices from road sections of highway 40. Highway 40 is one of the most important roads connecting the major cities of Saudi Arabia and the Gulf Countries. The road was uniformly divided into 1 km sections, and each section consists of 6 lanes (in both directions), as shown in Figure 1.

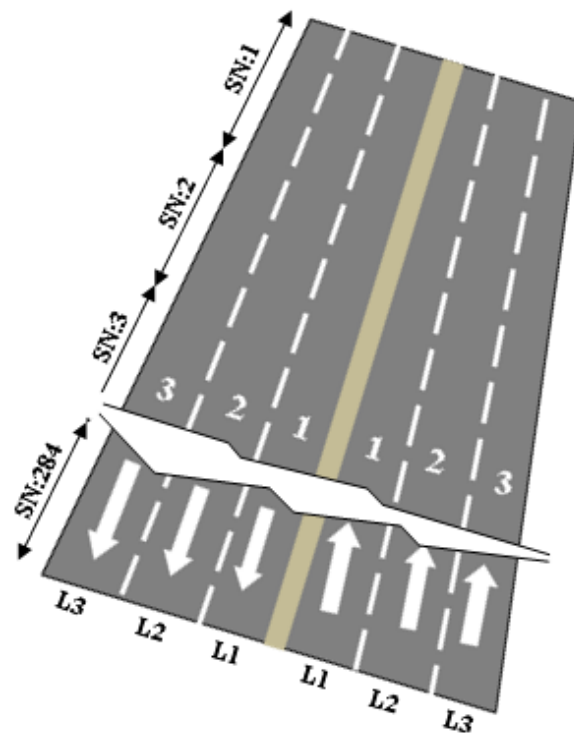


Figure 1. Sketch and Lane Numbering of 6-Lane Freeway.

The various lanes were abbreviated as follows: Lane 3 (L3), Lane 2 (L2), and Lane 1 (L1). A screen shot of a preprocessed typical lane data sheet is shown in Figure 2. Different direction for a given lane was signified by +1 and −1; hence each lane data sheet contains PC data for both directions (back and forth).

	A	B	C	D	E	F	G	H	I	J	K
1	DIR	SN	IRI	RUT	CI	TEXT	PSI	PCR	LAT	LON	
2	1	1	2.17	5.29	7.44	0.54	3.4	67.5	25.15131	47.57618	
3	1	2	1.8	4.55	7.12	0.58	3.63	100	25.1531	47.58584	
4	1	3	1.61	4.69	8.18	0.53	3.75	100	25.15337	47.59569	
5	1	4	1.83	3.39	6.9	0.6	3.72	100	25.15317	47.60566	
6	1	5	1.45	2.6	7.65	0.57	3.93	100	25.15251	47.61557	
7	1	6	1.2	2.3	8.92	0.52	4.04	100	25.15429	47.62521	
8	1	7	1.28	2.84	9.38	0.57	3.98	100	25.15884	47.6337	
9	1	8	1.58	3.3	7.96	0.58	3.77	100	25.16514	47.64082	
10	1	9	1.33	3.16	9.58	0.51	3.94	100	25.17053	47.64896	
11	1	10	1.71	3.17	6.07	0.86	3.7	100	25.17561	47.65714	
12	1	11	1.97	2.83	4.88	0.73	3.51	88	25.18043	47.66555	
13	1	12	2.18	3.61	3.66	0.87	3.4	68	25.18579	47.67354	

Figure 2. Typical Preprocessed Lane Pavement Condition Data Sheet.

2.1. Pavement Conditions and other Variables

This subheading gives a brief description of the abbreviated variables and PCs shown in the data sheet in Figure 2.

- A. **Direction (DIR):** this represents the direction of traffic movement either to or fro for a given lane. The two directions have been numerically represented by +1 (to) and −1 (fro).
- B. **Section Number (SN):** This column represents the section number for each lane. SN is more of a location-matching variable.
- C. **International Roughness Index (IRI):** IRI is a measure of longitudinal roughness of the road, and an indicator of ride quality, safety, and road user cost. The United State Federal Ministry of Highway and Administration (FHWA) recommends an acceptable range of IRI between 1.5 to 2.76 m/km [52]. Similar range and scaling of IRI is employed by highway agencies in Saudi Arabia [53]. Any road section with IRI below 1.5 m/km can be considered to be in good condition.
- D. **Pavement Rutting (Rut):** Pavement rutting is among the major road distresses that easily compromise the road's functional and structural integrity. It is the permanent depression that manifest longitudinally along vehicle wheel tracks on the road. There are three basic severity levels prescribed by the FHWA, Low (5–12 mm), Medium (12–25 mm) and High (>25 mm) rut distress levels. Anything below 5 mm is considered insignificant [54].
- E. **Crack Index (CI):** This represents the magnitude of cracks that manifested on the pavement surface at the time of evaluation. It is the function of the various types of cracks (transverse and longitudinal), and the percentage of area covered by these cracks and their severities.
- F. **Pavement Texture (Tex):** is the measure deviation of the road surface from an ideal smooth plane and is accurately measured with laser technology. It affects the tire–pavement interaction such as skid and rolling resistance. Pavement texture influences the amount of noise generated by moving vehicles, as well as driver's safety and vehicle fuel efficiency.
- G. **Present Serviceability Index (PSI):** Is a measure of pavement serviceability rating developed by AASHTO, which was later mathematically correlated to pavement distresses and roughness [55]. The original mathematical model for estimating PSI of flexible pavement is given by (1). PSI value of 5.0 signifies new and perfect pavement. This value declines with age of pavement due to defects and degradation, prompting the need for major maintenance at around PSI values of 3.0–2.0.

$$PSI = 5.03 - 1.91 \log_{10}(1 + \overline{SV}) - 1.38 * \overline{Rut}^2 - 0.01 \sqrt{(C + P)} \quad (1)$$

where \overline{SV} is the slope variance and a function IRI (in/mile), \overline{Rut} is the average rut depth, and $(C + P)$ is the sum of total cracked and patched area in $ft^2/1000ft^2$ of the pavement.

- H. **Pavement Condition Rating (PCR):** The PCR is an overall pavement condition rating that also depends on other indices such as the roughness condition index (RCI), and Surface Condition Rating (SCR) [54]. Road sections with PCR values below 60 are considered to have failed. According to FHWA methodology, PCR, RCI, and SCR can be estimated from Equations (2)–(5), respectively.

$$PCR = 0.6 * SCR + 0.4 * RCI \quad (2)$$

$$RCI = 32 \left[5 \left(2.718282^{(-0.0041IRI)} \right) \right] \quad (3)$$

$$SCR = 100 - [(100 - 10 * CI) + (100 - Rut_{index})] \quad (4)$$

$$Rut_{index} = 100 - 40 \left[\frac{\%Rut_{low}}{160} + \frac{\%Rut_{medium}}{80} + \frac{\%Rut_{high}}{40} \right] \quad (5)$$

The values $\%Rut_{low}$, $\%Rut_{medium}$, and $\%Rut_{high}$ reported the percentage of the 20 measurements within that severity.

- I. **Longitude (LON):** is the geographical longitude bearing coordinate for that particular road section.
- J. **Latitude (LAT):** is the geographical latitude bearing coordinate for that particular road section.

2.2. Data Analysis and Modeling

Basic statistics of the various road indices were estimated and compared lane-wise. Correlation of these road indices between lanes was also estimated in terms of Pearson correlation. Lane 3 was considered the most damaged and critical lane due to its usual extreme PC (see Table 1). Thus, it was selected as a predicting lane because the lane with the worst PC will always be a priority for accurate PC measurement, and timely maintenance. Since L3 indices are the selected predicting variables of other lanes indices, the correlations between the various road condition indices of L3 were also estimated and analyzed. Welch 2 sample t-test was utilized at a 5% significance level to evaluate whether the PC of adjacent lanes differs significantly or otherwise. Unlike classical t-test, the Welch t-test is insensitive to unequal variance for all sample sizes [56]. The null hypothesis (H_0) assumes the PCs of two adjacent lanes are the same, while the alternative hypothesis (H_a) assumes the PCs of two adjacent lanes are significantly different. Stepwise MLR (MLR) was then used to develop predictive models of L2 and L1 road condition indices in terms of L3 indices. Stepwise MLR systematically adds or removes a variable to the predicting model based on whether it improves or lessens the model performance. MiniTab16™ standard stepwise regression module was employed to generate simple MLR model of all L2 and L1 indices. A value of 0.15 α -to-enter and α -to-remove was used. Due to unsatisfactory model performance, MATLAB stepwiselm stepwise regression function was also used to establish quadratic models with interactive terms of L2 and L1 indices. Starting from a constant model, stepwiselm uses forward and backward stepwise regression to determine a final model. At each step, the function searches for a term to add to or remove from the model based on the selection criteria. Finally, ANN models were trained and developed using MATLAB application. The partitioning for training/testing of 70/30 of data set was utilized.

Table 1. Road Condition Indices Statistics, correlations between Indices of other Lanes and Lane 3, and t-test of adjacent lanes PCs.

PC	Statistics of Various Lanes Conditions Indices				Correlation with Lane 3 Conditions Indices			Two Samples <i>t</i> -Test between PCs of Adjacent Lanes			
	Para-Meter	Lane 3	Lane 2	Lane 1	Terms	L2	L1	Terms	L1/L2	L1/L3	L2/L3
IRI (m/km)	Mean	2.05	1.36	1.56	<i>R</i>	0.253	0.324	<i>t</i> -value	7.370	−12.55	−19.79
	St. Dev.	0.74	0.36	0.54	DF	566	566	DF	989	1038	823
	Min.	0.91	0.65	0.72	<i>p</i> -value	0.000	0.000	<i>p</i> -value	0.000	0.000	0.000
	Max.	7.44	3.05	3.39							
Rut (mm)	Mean	5.48	4.15	4.33	<i>R</i>	0.299	0.196	<i>t</i> -value	2.040	−8.780	−46.47
	St. Dev.	2.55	1.18	1.81	DF	566	566	DF	975	1024	573
	Min.	1.75	1.76	1.35	<i>p</i> -value	0.000	0.000	<i>p</i> -value	0.042	0.000	0.000
	Max.	20.73	8.86	15.04							
CI	Mean	7.04	8.08	7.67	<i>R</i>	0.406	0.382	<i>t</i> -value	−3.600	4.620	7.660
	St. Dev.	2.63	1.90	1.93	DF	566	566	DF	1133	1041	1033
	Min.	0.08	1.15	1.18	<i>p</i> -value	0.000	0.000	<i>p</i> -value	0.000	0.000	0.000
	Max.	10.00	10.00	10.00							
Texture (mm)	Mean	0.71	0.51	0.58	<i>R</i>	−0.029	0.191	<i>t</i> -value	7.660	−12.660	−17.71
	St. Dev.	0.20	0.20	0.14	DF	566	566	DF	1028	1038	1133
	Min.	0.36	0.26	0.27	<i>p</i> -value	0.484	0.000	<i>p</i> -value	0.000	0.000	0.000
	Max.	1.73	1.4	1.16							
PSI	Mean	3.53	3.93	3.81	<i>R</i>	0.281	0.357	<i>t</i> -value	−7.170	12.830	21.170
	St. Dev.	0.39	0.24	0.34	DF	566	566	DF	1016	1118	949
	Min.	1.42	2.99	2.78	<i>p</i> -value	0.000	0.000	<i>p</i> -value	0.000	0.000	0.000
	Max.	4.24	4.45	4.4							
PCR	Mean	78.43	93.79	88.81	<i>R</i>	0.221	0.304	<i>t</i> -value	−6.570	9.470	15.200
	St. Dev.	21.64	10.60	14.64	DF	566	566	DF	1033	996	824
	Min.	12.50	45.00	32.50	<i>p</i> -value	0.000	0.000	<i>p</i> -value	0.000	0.000	0.000
	Max.	100.00	100.00	100.00							

2.3. Neural Network (NN) Modeling

A two-layer (excluding the input) feed forward NN was coded in MATLABTM (R2017a). Although ANN models are categorized as black boxes due to low interpretability of model structure, they yield astounding prediction performance compared to conventional modeling techniques [57,58]. The architecture of the NN utilized in this study is presented in Figure 3. All ten indices of L3 were considered as input to predict PC index of L2 or L1. Sensitivity analysis was later conducted to assess which of the variables played more significant role in the model performance. Attempt was made to create NN models with two out puts (L2 and L1 indices), but the resulting models' accuracies were comparably lower than those of single out put models. *S* represents the number of neurons in layer 1, and varies for the various predicted indices. The weight and bias matrices are denoted by *W* and *b*, respectively. The transfer function f^1 is a hyperbolic tangent sigmoid equivalent function given by (5). Each of the variables from the input matrix *X*, is connected to each neuron through the weight matrix *IW*. In this case, a^1 is a 10-element column vector formed by " f^1 " from the weighted sum of the input variables x_i and bias b_i of the neurons' outputs. The neurons' outputs serve as inputs to f^1 , which transforms inputs to fall between the interval of [−1, 1]. The second layer function ' f^2 ' is a linear transfer function that normalizes the outputs from f^1 , which is then reversed by Equation (6), to be compared to the target output ' y_{a_i} '. Due to the random nature of the data, Bayesian Regularized (BR) Levenberg–Marquardt optimization was selected as the training algorithm [59,60]. The Bayesian Regularized Neural Networks are difficult to over-train, over-fit, and validation process is unnecessary [61]. The model performance is evaluated in terms of Mean Square Error (MSE) given by Equation (8), and coefficient of correlation (R^2) between actual and predicted PC given by Equation (9). However, for easy assessment and evaluation of

model accuracy, the Root Mean Square Error (RMSE) of the training and testing outputs was reported. Number of neurons for each model was optimized based on lowest and highest obtainable MSE and R^2 values, respectively. Balanced performance output between training and test data set was ensured by randomly reshuffling training/test data sets until approximately equal MSE and R^2 are obtained.

$$f^A(t) = 2 / (1 + e^{-2t}) - 1 \tag{6}$$

where t is the independent variable and e is the natural log base constant (2.718281).

$$y(r) = \frac{(y_{max} - y_{min})(r - r_{min})}{(r_{max} - r_{min})} + y_{min} \tag{7}$$

where r is a finite real number ranging between $[-1, 1]$, y_{max} and y_{min} are the maximum and minimum values of the original target data set, respectively.

$$MSE = (RMSE)^2 = \frac{\sum_i^{n_t} (y_{a_i} - y_p(u_i))^2}{n_t - n_p} \tag{8}$$

$$R^2 = 1 - \frac{\sum_i^{n_t} (y_{a_i} - y_p(u_i))^2}{\sum_i^{n_t} (y_{a_i} - \bar{y}_a)^2} \tag{9}$$

where $RMSE$: root mean square error, y_{a_i} : actual observed ARAs, $y_p(u_i)$: modeled or predicted ARAs, n_t : total number of observed ARA, n_p : number model parameters, \bar{y}_a : mean of observed ARA (Figure 3).

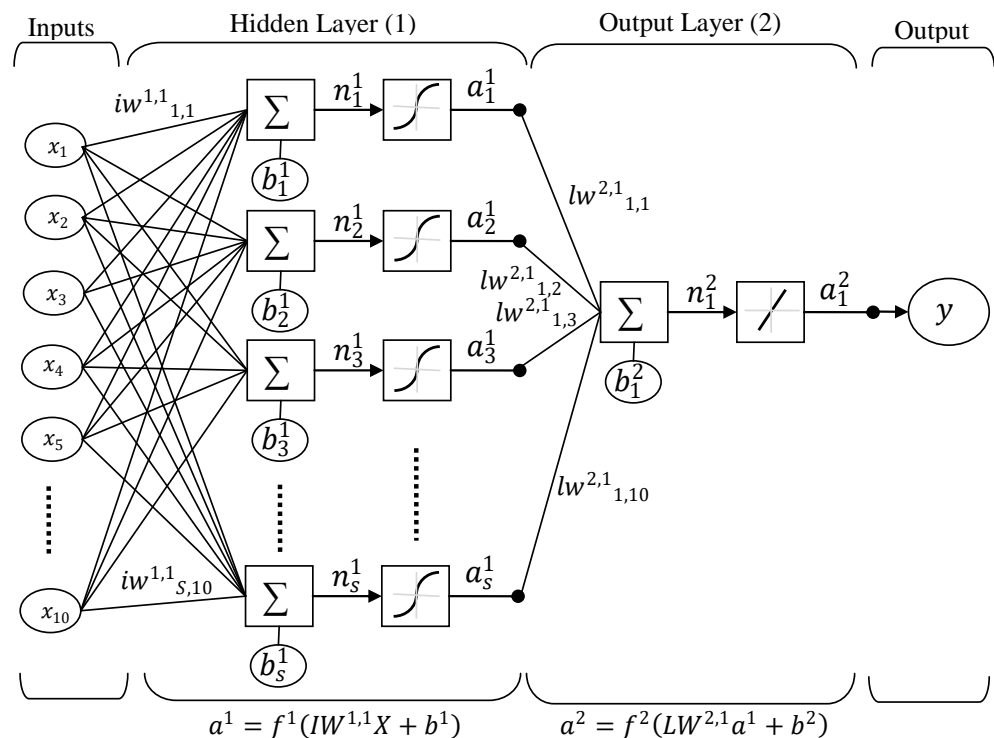


Figure 3. ANN Models Architecture.

Sensitivity Analysis of ANN Models

The model performance decomposition method was utilized to evaluate the sensitivity of the ANN models to the PC-predicting variables. The partial contribution of each PC predicting variable to the model performance was obtained by excluding that variable

from the final general model [62]. In this study, the partial performance of each variable was estimated by retraining the same model, with same number of neurons, but with the exclusion of that variable. At least three model performance outputs for each variable exclusion were generated by randomly reshuffling the training, and test partition 3 times. Average values of RMSE and the R^2 resulting from both training and testing were reported as the final results. Percent decrease or increase in RMSE and R^2 with respect to the original RMSE and R^2 were estimated according to Equations (10) and (11), respectively.

$$\% \Delta RMSE_n^m = \frac{RMSE_n^m - RMSE_o^m}{RMSE_o^m} \quad (10)$$

$$\% \Delta R_n^2 = \frac{R_n^2 - R_o^2}{R_o^2} \quad (11)$$

$n = 1, 2, \dots, 10; m = 1, 2, \dots, 12.$

$\% \Delta RMSE_n^m$ Represents the percent change in RMSE after exclusion of n^{th} predicting variable from m^{th} ANN PC model. $RMSE_n^m$ Denotes the final average RMSE after exclusion of n^{th} predicting variable from m^{th} ANN PC model. $RMSE_o^m$ Represents the original RMSE of the m^{th} ANN PC model including all 10 predicting variables. The terms in Equation (11) hold similar meaning as in Equation (10), but with R^2 as a replacement of RMSE.

3. Results and Discussion

3.1. Variables Selection

The basic statistics of the PC indices for the various lanes is summarized in Table 1. It can be seen that lane 3 (L3) is having the worst PCs and thus the critical lane. This is obviously due to traffic characteristics that are common on L3. In Saudi Arabia and several other countries around the world, L3 (outer lane) is prescribed for heavy trucks. In addition, most slow-moving vehicles are recommended, and they choose to travel on L3. The combination of heavy load and slow traffic is more detrimental to flexible pavement, than high speed and numerous low-load traffic. These are some of the reasons why the pavement of lane 3 showed higher average rutting, roughness, and texture, in addition to lower PSI and PCR. Sample plots showing the variation of IRI and PSI along the road length for L3 against lane 2 and lane 1 are shown in Figure 4. It can be observed that L3 showed higher IRI and lower PSI in most part of the road compared to the other lanes. Considering that poorer PC is a priority for maintenance intervention, and might require better and more accurate PC evaluation, the PC indices of L3 are selected as the predictors of Lane 2 (L2) and Lane 1 (L1) PC indices. It is also worth noting that although the PC plots vs. the road length appeared to be highly nonlinear, the road length is not the predicting variable, the PC indices of the adjacent lane are (PCs of L3). These PC indices also vary non-linear along the road length and in a similar pattern as the target PCs (for L1 and L2). These facts make the problem relatively less nonlinear, and give the MLR a chance.

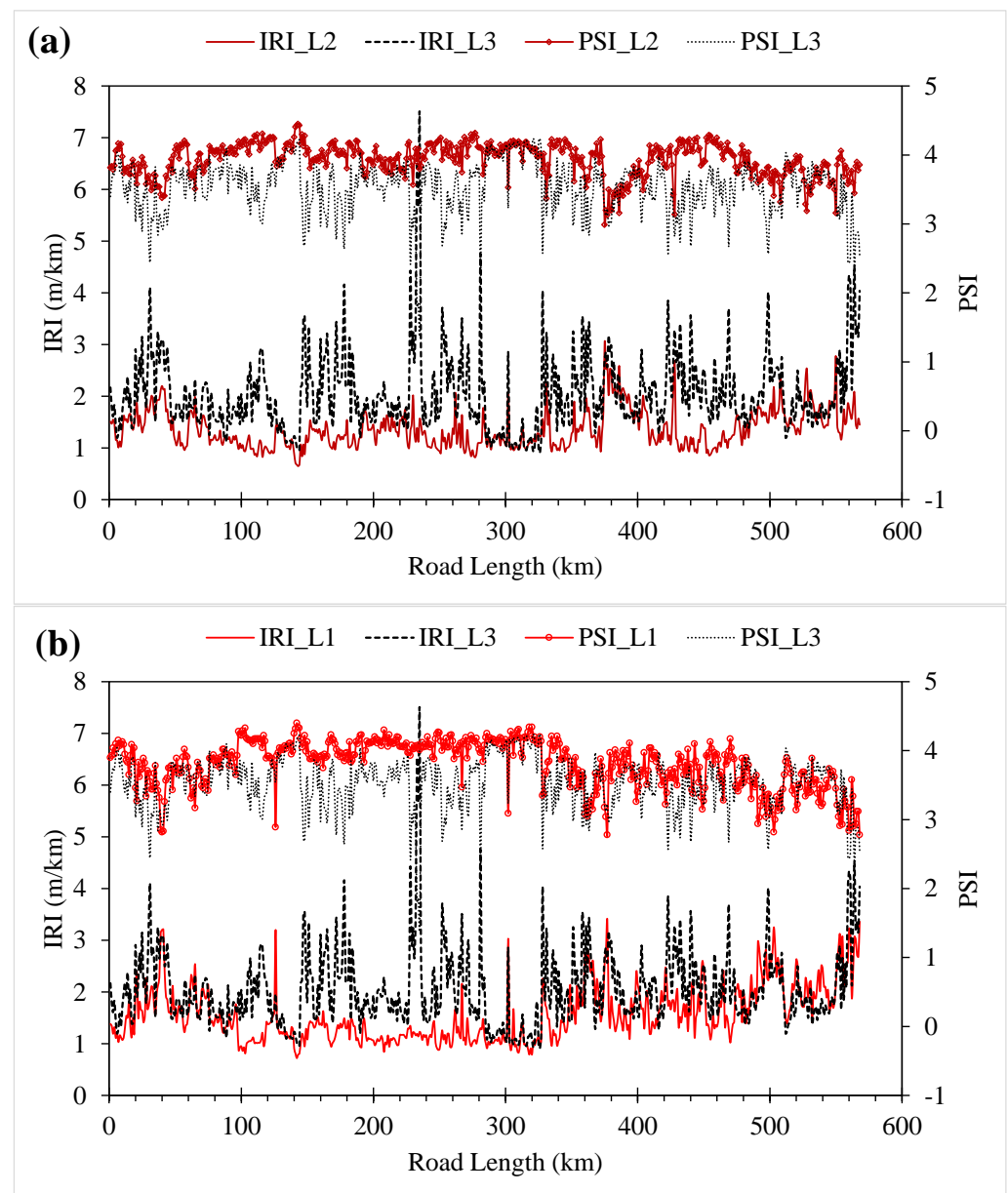


Figure 4. IRI and PSI Plots of (a) Lane-2 vs. Lane-3, and (b) Lane-1 vs. Lane-3.

The correlations of L3 PC indices with L2 and L1 indices are also presented in Table 1. Parameter of the correlation analysis includes Pearson correlation coefficient (R^2), Degree of Freedom (DF), and p -value. Almost all of the PCs of L2 and L1 (with the exception of Texture for L2) showed statistically significant but weak correlations with the PCs of L3. Some of the PCs showed higher correlations with L3 PCs than others. The existence of these correlations can be anticipated for several reasons. These reasons include materials, construction, and sub-grade variables which are most likely common to adjacent lane of a given road section. Traffic volume and distribution between lanes are usually not the same but are consistent with time. However, the surprisingly low correlations between the lanes' PC indices indicate the absence of a simple explicit mathematical relationship between them. Hence in which case the use of non-conventional AI modeling techniques such as ANN might be necessary. Two-sample t -test results of comparison between similar PCs of the various lanes is also shown in the last columns of Table 1. It can be seen that all similar PCs of the various lanes are significantly different from each other (p -value < 0.05). This implies that the observed differences in mean values and margins between individual PCs for different lanes in Table 1 and Figure 4, respectively, are statistically significant.

The correlation between the predicting variables (L3 PC indices) was estimated and presented in Table 2. One out of highly correlated variables can be adopted instead of them all in a regular regression analysis. However, stepwise regression employed in this study automatically takes care of this issue by only adding variables that improve the model's performance. The indices showing statistically significant and meaningful correlations are highlighted in red font. The IRI, Rut, CI, and Texture are fundamental PCs obtained directly from the pavement. Any correlation observed between these PCs and with other variables such as 'Dir' is not mathematically explicit. Other PC indices such as PSI, and PCR are secondary variables that are indirectly related to some of the primary PCs as discussed in Section 2.1. Correlations such as that between PSI and other fundamental PCs were only later established empirically. However, PSI was earlier a direct outcome of ride experience evaluation from panel of observers, and was originally a direct measurement of ride quality. Other than these, the remaining variables such as the matching parameters did not show a significant relationship with one another. Overall, the main goal is to assess the potential and extent of these variables contribution in achieving the objective of this study.

Table 2. Correlations between Condition Indices of Lanes 3.

	Dir.	SN	IRI	Rut	CI	Tex	PSI	PCR	LON.
SN	0.000 1.000								
IRI	0.034 0.425	−0.082 0.051							
Rut	0.005 0.912	0.205 0.000	0.528 0.000						
CI	−0.177 0.000	0.394 0.000	−0.619 0.000	−0.191 0.000					
Tex	0.457 0.000	−0.074 0.078	0.459 0.000	0.136 0.001	−0.633 0.000				
PSI	−0.036 0.389	0.129 0.002	−0.986 0.000	−0.555 0.000	0.646 0.000	−0.450 0.000			
PCR	−0.076 0.070	0.079 0.061	−0.869 0.000	−0.605 0.000	0.727 0.000	−0.522 0.000	0.884 0.000		
LON.	0.000 1.000	0.998 0.000	−0.075 0.074	0.214 0.000	0.392 0.000	−0.070 0.096	0.122 0.004	0.073 0.081	
LAT.	0.000 1.000	1.000 0.000	−0.083 0.047	0.202 0.000	0.395 0.000	−0.076 0.072	0.131 0.002	0.080 0.057	0.997 0.000

Cell Contents: Pearson correlation (R); *p*-Value.

3.2. Simple Multiple Linear Regression (S-MLR) Models

Simple MRL models of L2 and L1 PC indices in terms of those of L3 were first developed and assessed. These models are linear combinations of L3 indices and can be generally written as an Equation (12). The coefficients and corresponding *p*-values are summarized in Table 3. It can be observed that not a single model contains all the available variables. Some were better off with only 4 of the 10 initial variables. The most frequently appeared variables on the various models are IRI, PSI, Texture, and Direction. The second most relevant predicting variables are CI and location matching parameters (SN and LON). Rut and PCR played overall little role in supporting the various PC indices predictive models. Almost all of the included independent variables tend to be significantly relevant to the predicting model performance (at 5% significant level). The lack of significance of some the

predicting PC variables is not unrelated with the inability of MLR to adequately capture the nonlinear trend of the various conditions observed earlier (as seen Figure 4). This is because overall, the performances of the various models can be rated as poor in terms of R² values. However, the Root Mean Square Errors (RMSE) for some of the models appeared to be within reasonable ranges. The results of IRI and PSI models showed relatively the high and low R² values for lane 1 and lane 2, respectively. For this reason, the plots of predicted IRI and PSI of L1 and L2 models against their actual values are selected for visual examination.

$$Y_L^m = I_L^m + \sum_{n=1}^N C_n^m X_n^m \tag{12}$$

where Y_L^m is lane L pavement index m , $L = 2$ or 1 , and $m = 1, 2 \dots 6$ for the different distress or index types. I_L^m : intercept for lane L and PC index m . C_n^m and X_n^m are the coefficients and predicting variables, respectively. n is an integer number of the independent variables from L3 and varies from 1 to 10.

Table 3. Simple MLR Models for Lane 2 and Lane 1 Distresses and PCIs in terms of Lane 3 Distresses and PCIs.

Variables	IRI		Rut		CI		Texture		PSI		PCR	
	Lane 2	Lane 1	Lane 2	Lane 1	Lane 2	Lane 1	Lane 2	Lane 1	Lane 2	Lane 1	Lane 2	Lane 1
INTERCEPT	9.616	160.640	-454.000	1439.030	7.389	7.389	-39.18	-0.483	-1.908	-541.390	3197.500	-7102.730
DIR	-0.101 0.000	-0.225 0.000	0.138 0.006		0.385 0.000	0.385 0.000			0.069 0.000	0.144 0.000	1.050 0.011	4.970 0.000
SN		0.025 0.031	-0.079 0.000	0.256 0.000			-0.007 0.000			-0.095 0.049	-124.200 0.000	-1.240 0.001
IRI	-0.27 0.018	-0.250 0.063	-0.799 0.036	0.260 0.066	-0.820 0.000	-0.820 0.000	-0.109 0.103		0.178 0.016	0.180 0.031		
RUT			0.114 0.000	0.062 0.066			-0.023 0.000					
CI	0.0282 0.001		0.060 0.035	-0.240 0.000	0.352 0.000	0.352 0.000	0.033 0.000	0.022 0.000	-0.020 0.001			
TEX	0.29 0.005		0.800 0.018	-1.680 0.000	1.630 0.002	1.630 0.002	0.198 0.000	0.333 0.000	-0.214 0.002			-7.900 0.020
PSI	-0.430 0.000	-0.906 0.001	-1.350 0.079				-0.320 0.018		0.520 0.000	0.616 0.000	6.600 0.000	10.300 0.000
PCR					-0.016 0.026	-0.016 0.026						
LAT	-1.51 0.000	-3.259 0.016		-30.120 0.000					1.060 0.000	9.397 0.033		150.450 0.001
LON	2.65 0.000		18.400 0.000				1.620 0.000	0.026 0.127	-1.850 0.000	3.800 0.124	-124.200 0.000	
RMSE	0.312	0.380	1.020	1.620	1.620	1.620	0.179	0.132	0.205	0.253	9.840	12.200
R ² (%)	26.640	51.320	26.240	20.970	27.660	27.660	20.250	16.110	28.720	53.770	14.470	31.060

Note: 1st Cell Content is a Coefficient, while the 2nd Cell Content is its Corresponding p -value.

The predicted vs. actual plots showing margin of error for IRI and PSI of L1 and L2 are shown in Figure 5a,b, respectively. The RMSE of the IRI-L1, IRI-L2, PSI-L1, and PSI-L2 plots are 0.380 m/km, 0.312 m/km, 0.253, and 0.205, respectively. These values are not too high if the intervals of the IRI or PSI needed to classify a pavement section as acceptable or otherwise are considered. However, these level or errors cannot be accepted practically because they are associated to high uncertainties. This can be observed from the various margin of error between true and predicted IRI/PSI in the plots. Although most of the predicted values showed reasonably low deviations from the true values, a significant amount of the pavement sections that have an unacceptable level of IRI or PSI were predicted to be in good condition. The correlation coefficients of the various plots for IRI-L1, IRI-L2, PSI-L1, and PSI-L2 are 0.551, 0.266, 0.537, and 0.287, respectively. The R² values give insight into the generality of the prediction models. The more R² is closer to unity the more general the model. For example, the RMSE observed might have

downplayed the deficiencies of the various models, but the true and predicted correlation coefficients showed how these models become more inaccurate at extreme ends of the ranges of the utilized data. This was why the models could not capture the IRI and PSI at the extreme peaks and troughs of the plots. Significant difference in error margin could not be visually observed between plot in Figure 5a,b for L2 and L1, respectively. This because although IRI and PSI models of L2 showed lower R^2 than those of L1, the models of L2 possessed lower RMSE than those of L1. Similar plots of CI vs. Texture and Rut vs. PCR for L1 and L2 are presented in the Appendix A as Figures A2 and A3, respectively, for further information.

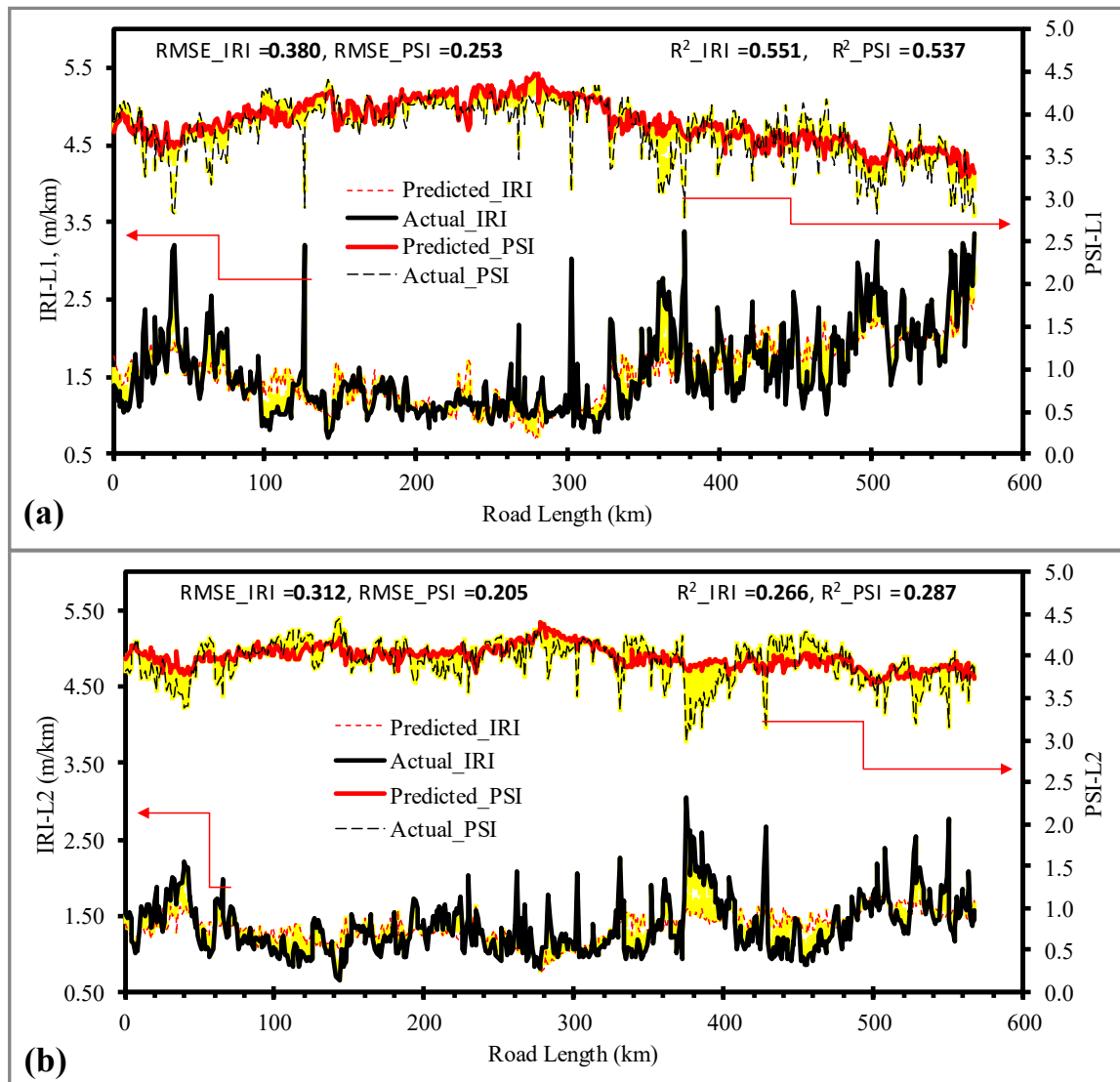


Figure 5. MLR Models Plots, Predicted vs. Actual with Margin of Error (Yellow) for (a) Lane-1 IRI and PSI, and (b) Lane-2 IRI and PSI.

The Q-MLR model were obtained using a different stepwise regression function in MATLAB (stepwiselm) which allows for automatic inclusion of interactive and higher order terms. The resulting Q-MLR models for L2 and L1 indices as a function of L3 PC indices are presented in Tables 4 and 5, respectively. The inclusion of interactive and higher order terms in to the MLR models certainly improved both the RMSE and R^2 significantly. However, the numerous interactive and squared terms have also made the regression equations lengthy and more complex. Unlike in the case of the S-MRL, all of the predicting variables played a significant role in the model, either alone or by interacting with other

variables. This confirms the previous hypothesis that the linear nature of the S-MLR models was partly responsible for the previous insignificant roles of some of the PC predicting variables. Figure 6 shows the various percent improvements in RMSE and R² values of Q-MLR models relative to S-MLR models. Although such relative improvement was observed, the various Q-MLR PC indices models are far from adequately accurate for practical PCs predictions. This is because none of the Q-MLR models could explain up to 70% of the observed PC data (R² < 0.7). This is despite the fact that 100% of the PC data were utilized for the regression analysis and model evaluation. It can thus be safe to say that these types of MLR regression models cannot adequately be relied upon to predict the PC indices of lanes as a function of adjacent lane PC variables. The ANN models were developed and analyzed in the next sub-heading.

Table 4. Quadratic MLR Models for Lane 2 Distresses and PCIs in terms of Lane 3 Distresses and PCIs.

	IRI	RUT	CI	TEX	PSI	PCR					
Intercept	−4,987.300	Intercept	142,670	Intercept	20,176,000	Intercept	−45376	Intercept	3,015,000	Intercept	82,971,000
DIR	−125.16	DIR	−3150.7	DIR	−8080	DIR	−0.41049	DIR	0.16871	DIR	−1787
SN	−1796.1	SN	−63.071	SN	7242.1	SN	−8.1093	SN	1088	SN	29745
IRI	−1495.4	IRI	−34.402	IRI	5248.8	IRI	205.56	IRI	753.53	IRI	−244.21
RUT	−167.96	RUT	−1839.2	RUT	−2466.2	RUT	10.78	RUT	101.67	RUT	4578.8
CI	126.08	CI	2307.9	CI	−2940.3	CI	−1.9882	CI	−75.117	CI	−9831.8
TEXT	−2.6151	TEXT	−7.1267	TEXT	−1557.5	TEXT	−559.03	TEXT	3577.6	TEXT	−8637.9
PSI	−4097.8	PSI	−23034	PSI	13531	PSI	4639.9	PSI	2285.7	PSI	−788.45
PCR	0.013807	PCR	−1.1581	PCR	0.075239	PCR	−64.256	PCR	21.961	PCR	−0.28437
LAT [†]	−321.9	LAT	−5651.5	LAT [†]	2072.8	LAT	431.17	LAT	295.17	LAT [†]	6178.2
LON	210,270	LON	−1316.2	LON	−849920	LON	1392	LON	−127230	LON	−3.49E+6
DIR*SN	−0.02308	DIR*SN	−0.56565	DIR*SN	−1.4426	DIR*SN	0.019799	DIR*SN	0.000421	DIR*SN	−0.32239
DIR*RUT	0.019773	DIR*IRI	−2.1524	DIR*CI	−0.1663	DIR*CI	0.014733	DIR*RUT	−0.01099	DIR*IRI	4.0006
DIR*CI	0.025276	DIR*CI	0.069223	DIR*TEXT	−1.4869	DIR*PSI	0.087773	DIR*CI	−0.01658	DIR*RUT	−0.72962
DIR*LON	2.6264	DIR*TEXT	1.0866	DIR*PSI	−0.73049	DIR*PCR	−0.00138	SN*IRI	0.13636	DIR*TEXT	−14.854
SN*IRI	−0.2717	DIR*PSI	−4.0427	DIR*PCR	0.020947	SN*IRI	0.03371	SN*RUT	0.018482	DIR*LAT	71.314
SN*RUT	−0.03028	DIR*LAT	34.174	DIR*LAT	88.569	SN*RUT	0.001762	SN*CI	−0.01353	SN*RUT	0.835
SN*CI	0.0228	DIR*LON	48.545	DIR*LON	123.12	SN*TEXT	−0.09894	SN*TEXT	0.63976	SN*CI	−1.7583
SN*PSI	−0.74352	SN*RUT	−0.32934	SN*IRI	0.95671	SN*PSI	0.82372	SN*PSI	0.41393	SN*TEXT	−1.4972
SN*LON	37.831	SN*CI	0.41268	SN*RUT	−0.43826	SN*PCR	−0.01153	SN*PCR	0.003931	SN*LON	−625.11
IRI*RUT	0.21897	SN*PSI	−4.1138	SN*CI	−0.52656	SN*LON	0.11956	SN*LON	−22.928	IRI*RUT	−9.5157
IRI*LON	31.431	SN*LON	1.6284	SN*TEXT	−0.28749	IRI*TEXT	−0.13412	IRI*PSI	−0.53833	IRI*TEXT	−70.028
RUT*PSI	0.40288	IRI*RUT	0.81057	SN*PSI	2.461	IRI*PCR	−0.00996	IRI*PCR	0.005349	IRI*PSI	−33.276
RUT*LON	3.4929	IRI*PSI	3.5644	SN*LON	−152.35	IRI*LAT	−8.1298	IRI*LON	−15.797	IRI*LAT	537.96
CI*TEXT	−0.18545	IRI*PCR	0.12325	IRI*RUT	−0.72298	RUT*LAT	−0.42999	RUT*PCR	0.000694	IRI*LON	−275.04
CI*LON	−2.6487	RUT*PSI	1.6857	IRI*LON	−110.34	CI*LAT	0.075479	RUT*LON	−2.1397	RUT*TEXT	−4.9425
TEXT*PSI	1.1011	RUT*LAT	15.962	RUT*TEXT	−0.50002	TEXT*LON	11.761	CI*TEXT	0.17722	RUT*PSI	−19.734
PSI*LON	86.12	RUT*LON	30.078	RUT*PSI	−1.287	PSI*PCR	−0.01954	CI*LON	1.577	RUT*LON	−94.358
LAT*LON	−422.22	CI*PCR	−0.00463	RUT*LAT	27.692	PSI*LAT	−60.652	TEXT*PSI	−1.1476	CI*PCR [†]	0.025864
SN ²	−0.16168	CI*LAT	−18.937	RUT*LON	37.342	PSI*LON	−65.448	TEXT*LAT	−27.244	CI*LAT	95.212
RUT ²	0.004667	CI*LON	−38.505	CI*TEXT	1.7894	PCR*LAT	0.64777	TEXT*LON	−60.759	CI*LON	156.46
PCR ²	−7E−05	TEXT*PSI	3.2312	CI*LAT	28.755	PCR*LON	1.0105	PSI*LON	−48.023	TEXT*PSI	−159.3
LAT ²	405.89	TEXT*PCR	−0.04669	CI*LON	46.586	LAT*LON	−48.206	PCR*LAT [†]	−0.2003	TEXT*LAT	371.74
LON ²	−2102.8	PSI*PCR	0.27703	TEXT*PCR	−0.12599	RUT ²	0.003019	PCR*LON [†]	−0.35671	PSI*LAT	1255.1
		PSI*LAT	200.85	TEXT*LAT	61.823	CI ²	0.005189	LAT*LON	254.55	PSI*LON	−632.04
		PSI*LON	377.26	PSI*LON	−284.48	LAT ²	41.075	SN ²	0.098126	LAT*LON	8997.2
		SN ²	−0.01585	LAT*LON	2196.8			IRI ²	−0.21842	SN ²	2.6657
		IRI ²	1.7593	SN ²	0.64983			PCR ²	0.00016	RUT ²	−0.33006
		RUT ²	0.010569	RUT ²	−0.02978			LAT ²	−246.04	CI ²	−0.42372
		LAT ²	98.395	CI ²	0.050773			LON ²	1273.2	PSI ²	−65.576
				TEXT ²	3.9505					LAT ²	−8763.1
				LAT ²	−2127.3					LON ²	34335
				LON ²	8361						
RMSE	0.251	RMSE	0.883	RMSE	1.18	RMSE	0.136	RMSE	0.163	RMSE	7.88
R ²	0.550	R ²	0.481	R ²	0.641	R ²	0.565	R ²	0.574	R ²	0.488

[†] Terms with *p*-values greater than 5%.

Table 5. Quadratic MLR Models for Lane 1 Distresses and PCIs in terms of Lane 3 Distresses and PCIs.

IRI		RUT		CI		TEX		PSI		PCR	
Intercept	−8.46E+5	Intercept	1.17E+06	Intercept	1.91E+07	Intercept	25485	Intercept	4.78E+5	Intercept	−8.17E+6
DIR	2351.9	DIR	12,584	DIR	−13,291	DIR	−36.78	DIR	−1546.8	DIR	−97,228
SN	−336.13	SN	209.75	SN	6734.2	SN	4.5142	SN	192.47	SN	−1459.8
IRI	−14152	IRI	−63747	IRI †	210.33	IRI	−1800.4	IRI	9275.1	IRI	5.16E+05
RUT †	0.028914	RUT	16.415	RUT	−131.95	RUT	−11.221	RUT	0.032893	RUT	−3.1127
CI	514.44	CI	5580.5	CI	−2332.4	CI †	−0.04181	CI	−322.88	CI	−30498
TEXT	34.105	TEXT	30,318	TEXT	−68.948	TEXT	0.20717	TEXT	−23.186	TEXT †	−9.0446
PSI	−30340	PSI	−1.29E+5	PSI	−70.68	PSI	−844.75	PSI	19,617	PSI	1.07E+06
PCR	0.05492	PCR	19.125	PCR †	0.051287	PCR	−46.454	PCR	−0.01366	PCR	0.34824
LAT	−1071	LAT	−30,601	LAT	−4482.7	LAT	−91.746	LAT	706.77	LAT	61,579
LON	38,885	LON	−22,145	LON	−8.00E+5	LON	−815.51	LON	−22,256	LON	2.15E+05
DIR*SN	0.42155	DIR*SN	2.2528	DIR*SN	−2.3769	DIR*SN	−0.00615	DIR*SN	−0.2772	DIR*SN	−17.417
DIR*PSI	0.20165	DIR*RUT	−0.06095	DIR*IRI	−2.1331	DIR*CI	0.009409	DIR*PSI	−0.10405	DIR*CI †	0.66789
DIR*LAT	−19.882	DIR*CI	−0.24414	DIR*TEXT	1.0249	DIR*TEXT	−0.09728	DIR*LAT	13.199	DIR*TEXT	15.479
DIR*LON	−38.961	DIR*TEXT	−1.3265	DIR*PSI	−4.1952	DIR*PSI	−0.04283	DIR*LON	25.557	DIR*LAT	863.97
SN*IRI	−2.5289	DIR*LAT	−112.04	DIR*LAT	122.24	DIR*LAT	1.4664	SN*IRI	1.6597	DIR*LON	1587.3
SN*RUT †	0.000218	DIR*LON	−205.3	DIR*LON	215.23	SN*IRI	−0.32222	SN*CI	−0.05776	SN*IRI	92.302
SN*CI	0.091863	SN*IRI	−11.396	SN*IRI †	0.042249	SN*RUT	−0.00181	SN*PSI	3.5099	SN*CI	−5.4612
SN*PSI	−5.4216	SN*CI	0.99706	SN*RUT	−0.02263	SN*CI	0.000164	SN*PCR	2.76E−05	SN*PSI	190.69
SN*LON	7.557	SN*TEXT	5.4247	SN*CI	−0.41771	SN*PSI	−0.15159	SN*LON	−4.3654	SN*LON	13.525
IRI*CI	0.043251	SN*PSI	−23.027	SN*TEXT	0.013858	SN*PCR	−0.00831	IRI*PSI	5.4178	IRI*PSI	185.71
IRI*TEXT	0.35699	SN*PCR	0.00337	SN*LON	−141.5	SN*LON	−0.05782	IRI*LAT	−78.607	IRI*LAT	−4117.7
IRI*PSI	−5.5782	SN*LAT	−3.8043	IRI*TEXT	8.1014	IRI*LAT	13.616	IRI*LON	−153.96	IRI*LON	−8691.9
IRI*PCR	−0.01062	SN*LON	−0.4314	IRI*PSI	3.5725	IRI*LON	30.656	RUT*TEXT	−0.06261	RUT*CI	0.31907
IRI*LAT	117.87	IRI*PSI	0.90405	IRI*LAT	−9.1198	RUT*LAT	0.44495	CI*LAT	2.586	CI*TEXT	7.5985
IRI*LON	235.76	IRI*PCR	−0.02732	RUT*LAT	5.2375	CI*PSI	0.020294	CI*LON	5.4216	CI*LAT	270.76
CI*LAT	−4.3628	IRI*LAT	576.37	CI*PCR	0.010846	PSI*LON	17.759	TEXT*LON	0.48347	CI*LON	497.84
CI*LON	−8.5112	IRI*LON	1035.6	CI*LAT	21.132	PCR*LAT	0.488	PSI*LAT	−166.16	TEXT*PCR	−0.65014
TEXT*LON	−0.71461	RUT*LON	−0.33256	CI*LON	37.856	PCR*LON	0.71871	PSI*LON	−325.72	PSI*LAT	−8548.4
PSI*LAT	254.15	CI*PCR	−0.00563	TEXT*PSI	15.214	LAT*LON	25.428	SN^2	0.019123	PSI*LON	−17,937
PSI*LON	504.69	CI*LAT	−50.147	LAT*LON	1833.4	CI^2	−0.00306	IRI^2	1.2164	LAT*LON	−536.53
SN^2	−0.03303	CI*LON	−90.813	SN^2	0.59347	LAT^2	−23.408	PSI^2	6.0535	IRI^2	42.418
IRI^2	−1.3801	TEXT*LAT	−282.47	TEXT^2	−2.8445			PCR^2†	5.14E−05	CI^2	0.46754
RUT^2	−0.00381	TEXT*LON †	−488.12	PSI^2	7.3199			LON^2	248.82	PSI^2	199.94
PSI^2	−6.2659	PSI*LAT	1199.2	PCR^2	−0.00083					LON^2	−1305.4
PCR^2	−0.00019	PSI*LON	2073.6	LAT^2	−1649.7						
LON^2	−431.7	PCR*LAT †	−0.75592	LON^2	7925.4						
		LAT*LON	543.29								
RMSE	0.323	RMSE	1.430	RMSE	1.190	RMSE	0.104	RMSE	0.200	RMSE	11.000
R²	0.668	R²	0.422	R²	0.642	R²	0.505	R²	0.680	R²	0.467

† Denotes Terms with p-values greater than 5%.

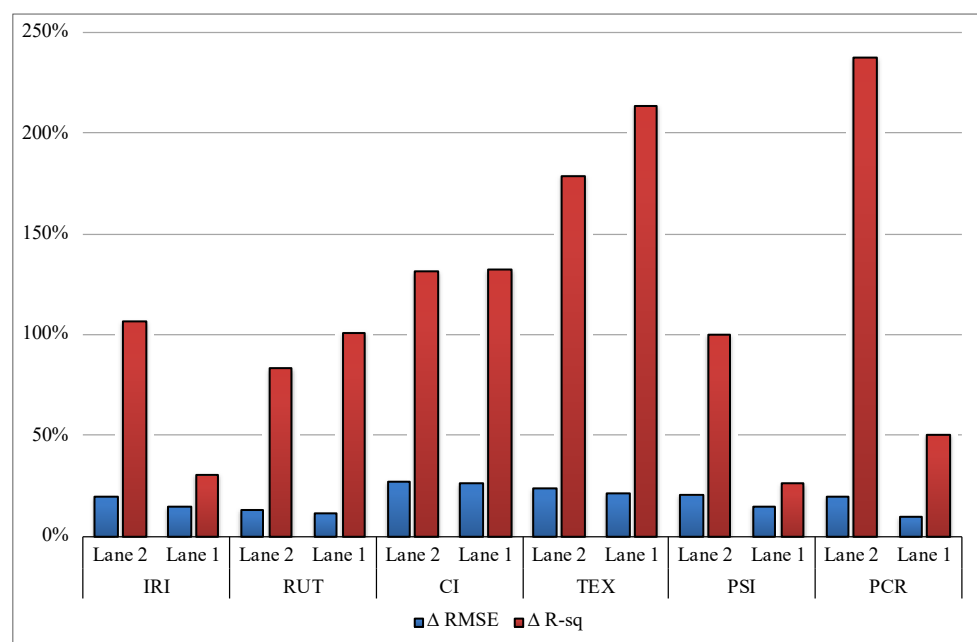


Figure 6. Percent Improvement in RMSE and R-sq from S-MLR to Q-MLR.

3.3. ANN Models

A summary of the ANN models' performances for the L2 and L1 PC indices is presented in Table 6. The number of neurons in the hidden layer is continuously adjusted until a reasonable balance between training and testing performance is achieved. Almost each PC index requires a different optimum number of neurons for a given lane. RMSE and correlation between the predicted and target PC for the training, testing, and combined (All) are listed. The corresponding training epochs at which these results were obtained were also presented. All PC model performance vs. epochs plots for training and test are shown in Figure A1, in Appendix A. The ANN models showed promising performances that indicates the possibility of evaluating a multi-lane highway PC by single lane inspection. All but the PCR model showed reasonable RMSE values, that are capable of explaining at least 80% of their various PC data ($R^2 \geq 0.8$), and some up to 90%. Poor performance of the PCR model is not unrelated to the semi-discrete nature of the PCR data which exhibited several wide flat peaks (see Figure A5 in Appendix A). Although PCR is and should be inherently continuous, it appears to rate several sections that are not significantly different as equals. This creates the numerous flat continuous peaks that ended up confusing the ANN algorithm. Unlike PCR, most other indices were able to account for the slightest variations between different road sections. The PCR prediction might yield better model performance if treated as a classification problem.

Table 6. Neural Network Models Performance Summary.

NN Modeling Results Summary of Lane 2 and Lane 1 Indices from Lane 3 Indices							
		Lane 2			Lane 1		
		Training	Testing	All	Training	Testing	All
IRI (m/km)	R ²	0.812	0.790	0.802	0.866	0.795	0.855
	RMSE	0.213	0.235	0.216	0.277	0.301	0.281
	Epoch		239	NA		462	NA
	Neurons		7			8	
Rut (mm)	R ²	0.818	0.782	0.800	0.782	0.780	0.781
	RMSE	0.684	0.834	0.708	1.151	1.023	1.133
	Epoch		237	NA		187	NA
	Neurons		10			8	
CI	R ²	0.908	0.911	0.908	0.891	0.893	0.892
	RMSE	0.801	0.776	0.797	0.858	0.960	0.874
	Epoch		133	NA		94	NA
	Neurons		9			8	
Texture (mm)	R ²	0.891	0.849	0.885	0.820	0.751	0.809
	RMSE	0.092	0.099	0.093	0.084	0.086	0.084
	Epoch		173	NA		117	NA
	Neurons		8			8	
PSI	R ²	0.807	0.791	0.805	0.879	0.850	0.874
	RMSE	0.144	0.137	0.143	0.165	0.174	0.167
	Epoch		356	NA		404	NA
	Neurons		7			10	
PCR	R ²	0.815	0.628	0.773	0.731	0.729	0.731
	RMSE	6.249	8.311	6.884	9.760	11.221	9.992
	Epoch		191	NA		235	NA
	Neurons		10			8	

ANN PC models similar to those visually analyzed previously (IRI and PSI models) from previous S-MLR models were also plotted for similar analysis. The lane 1 and lane 2 IRI and PSI ANN model plot for predicted vs. actual showing yellow error margin are presented in Figure 7a,b, respectively. The improvement in R² values of the ANN models

can be seen to be reflected in the lower level of deviation (yellow gap) of the predicted from the actual PSI and IRI values. This deviation was significantly higher in the S-MLR models (see Figure 5 for comparison). This is because, unlike the low R^2 values of the S-MLR model plots (0.551, 0.537, 0.2664, and 0.2872), the ANN models showed higher R^2 (0.855, 0.874, 0.802, and 0.805), for the Lane 1 IRI, Lane 1 PSI, Lane 2 IRI and PSI, respectively. The RMSE values for the IRI and PSI models have decreased from 0.380, 0.253, 0.312, and 0.205, to 0.281, 0.167, 0.216, and 0.143, respectively. The improvement in RMSE can be clearly observed as those seen for the R^2 , and their impact on margin of error is also visually significant. This is because, unlike in the case of S-MLR models, the number of excessively over and under predicted PC have decreased drastically, as can be observed from the predicted vs. actual plots in Figure 7. Similar plots of actual vs. predicted for CI with Texture, and Rut with PCR for L2 and L1 are presented in Figures A4 and A5, respectively, as further information in Appendix A.

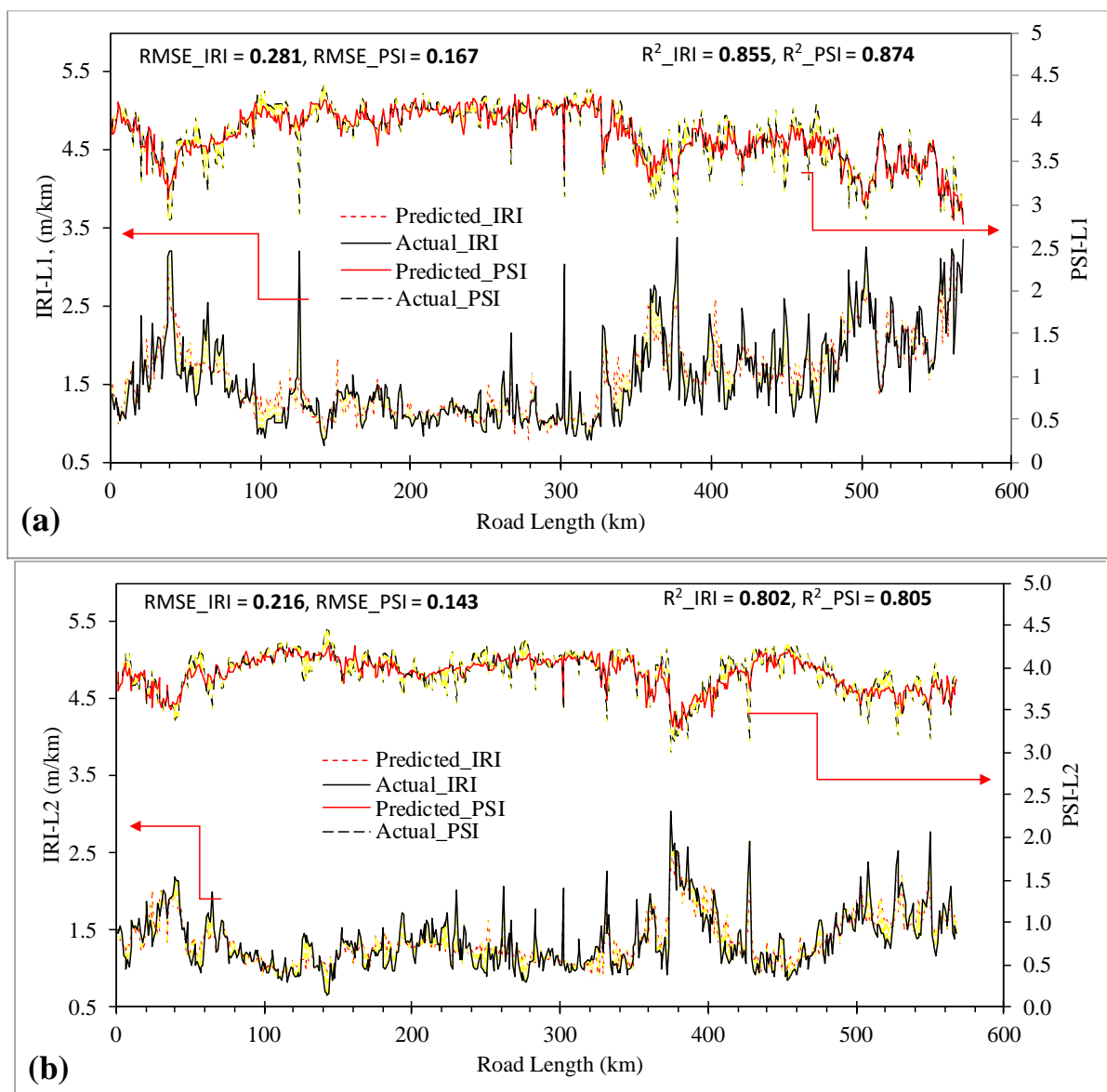


Figure 7. ANN Model Plots, Predicted vs. Actual with Margin of Error (Yellow) for (a) Lane-1 IRI and PSI, and (b) Lane-2 IRI and PSI.

Sensitivity Analysis of ANN Modeling Results

Percent change in RMSE and R^2 values of the IRI ANN models due to exclusion of individual predicting variables from the models are shown in Figure 8. This represents the relative influence of the variables with respect to the accuracy of the ANN model. A variable that results in a higher drop in the accuracy of the model is considered a crucial and influential factor in the model. It can be observed that exclusion of any of the predicting variable from the models of both L2 and L1 resulted in increase in RMSE and a decrease in R^2 value. However, the resulting change in RMSE was higher than that of R^2 value. The magnitude of the observed change in RMSE and R^2 for the different variables are also not the same for the different lanes. Increase in RMSE and decrease in R^2 is a clear indication of decrease in overall model performance. This implies that all the included predicting variables, i.e., the PC of L3, contributed positively in the IRI model performances of both L2 and L1. The traffic travel direction parameter 'Dir' contributed the most to the RMSE and the R^2 of the IRI ANN model. The traffic direction parameter 'Dir', the adjacent lane sections matching number (SN), and location parameter played a vital role, without which the data will be less meaningful to the ANN algorithm. This is because the PC variation between adjacent lanes, along the length of the road, and for different direction is not uniform (see Figure 4). Similar results of change in RMSE and R^2 value of other PC models for L2 and L1 are summarized and presented in Table 7. The average corresponding RMSE and R^2 values are presented in Appendix A in Table A1. Most of the observations made in the case of the IRI models are common to other PCs models, except PCR. Exclusion of a variable should either cause a decrease or an increase in the PCR model performance. The change in RMSE in the PCR models is also relatively low as compared to other PC models. This difference can be associated with the inability of the PCR model to perform as compared to the other PC indices. Excluding any predicting variable from the other PC models affects the model performance negatively. The negative effect of predicting variable exclusion can either be significant or less. The predicting variables were ranked according to their relative influence on the model performance, and the results is summarized in Table 8. The rank #1 represents the most influential, while rank #10 signifies least influential. The ranking was made on the absolute sum of change in RMSE and R^2 due to the exclusion of the variables. It can be observed that the traffic direction parameter consistently remained the most influential predictor for the PCs of both L2 and L1, with only the exception of PCR. Average or overall rankings for the different lanes PC models were obtained from the total absolute sum of changes in RMSE and R^2 due to variable exclusion. Due to inconsistent outcomes of PCR results as previously observed, results of PCR model were not included in the overall average ranking.

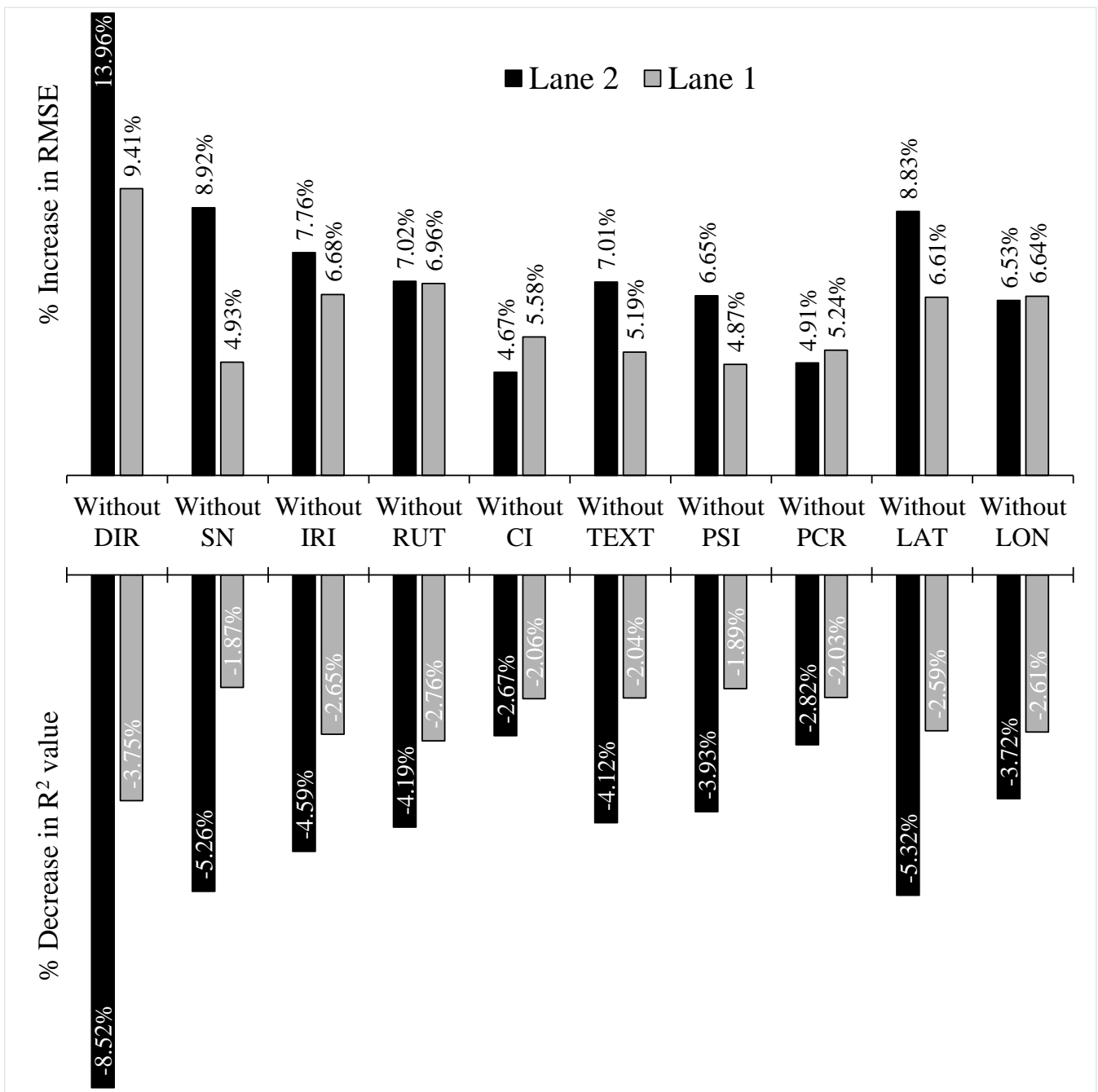


Figure 8. Percent Change in RMSE and R² after Variable Exclusion for IRI ANN Models.

Table 7. Summary of % Change in RMSE and R² after Variable Exclusion for All PC ANN models.

% Change in RMSE											
PC	Lane ID	Without DIR	Without SN	Without IRI	Without RUT	Without CI	Without TEXT	Without PSI	Without PCR	Without LAT	Without LON
IRI	Lane 2	13.96%	8.92%	7.76%	7.02%	4.67%	7.01%	6.65%	4.91%	8.83%	6.53%
	Lane 1	9.41%	4.93%	6.68%	6.96%	5.58%	5.19%	4.87%	5.24%	6.61%	6.64%
RUT	Lane 2	20.93%	9.24%	8.56%	6.60%	12.37%	12.66%	7.44%	8.54%	9.15%	10.07%
	Lane 1	13.90%	3.57%	3.78%	8.99%	6.17%	7.90%	3.95%	6.84%	6.19%	4.22%
CI	Lane 2	24.58%	3.58%	7.20%	5.78%	12.64%	8.22%	5.15%	1.48%	7.41%	7.07%
	Lane 1	21.81%	6.22%	8.15%	8.21%	4.95%	6.15%	2.36%	7.84%	6.10%	2.31%
TEXT	Lane 2	18.26%	7.57%	1.74%	1.74%	6.12%	3.40%	4.83%	2.86%	7.81%	0.75%
	Lane 1	18.49%	5.48%	4.82%	5.37%	10.23%	10.02%	3.92%	5.57%	7.75%	5.74%
PSI	Lane 2	8.59%	5.41%	4.64%	2.54%	7.10%	3.70%	5.04%	4.62%	6.97%	4.72%
	Lane 1	23.12%	8.32%	5.63%	11.90%	6.98%	6.37%	8.23%	6.05%	5.75%	7.35%
PCR	Lane 2	−1.72%	1.06%	0.74%	0.78%	−0.63%	−2.29%	−3.39%	−3.26%	2.05%	−2.41%
	Lane 1	2.15%	3.20%	−3.15%	3.77%	−2.90%	−2.37%	−2.07%	1.28%	−2.16%	0.34%
% Change in R ²											
PC	Lane ID	Without DIR	Without SN	Without IRI	Without RUT	Without CI	Without TEXT	Without PSI	Without PCR	Without LAT	Without LON
IRI	Lane 2	−8.52%	−5.26%	−4.59%	−4.19%	−2.67%	−4.12%	−3.93%	−2.82%	−5.32%	−3.72%
	Lane 1	−3.75%	−1.87%	−2.65%	−2.76%	−2.06%	−2.04%	−1.89%	−2.03%	−2.59%	−2.61%
RUT	Lane 2	−14.26%	−5.60%	−5.12%	−3.97%	−7.66%	−7.86%	−4.42%	−5.16%	−5.45%	−6.09%
	Lane 1	−10.09%	−2.38%	−2.52%	−6.28%	−4.17%	−5.41%	−2.65%	−4.70%	−4.17%	−2.82%
CI	Lane 2	−6.09%	−0.80%	−1.58%	−1.29%	−2.89%	−1.86%	−1.15%	−0.34%	−1.64%	−1.61%
	Lane 1	−6.48%	−1.73%	−2.27%	−2.25%	−1.33%	−1.68%	−0.65%	−2.20%	−1.65%	−0.60%
TEXT	Lane 2	−5.70%	−2.24%	−0.45%	−0.44%	−1.77%	−0.91%	−1.44%	−0.83%	−2.15%	−0.22%
	Lane 1	−11.38%	−2.99%	−2.66%	−2.96%	−5.89%	−5.78%	−2.20%	−3.13%	−4.42%	−3.26%
PSI	Lane 2	−5.04%	−3.10%	−2.66%	−1.47%	−4.14%	−1.96%	−2.91%	−2.56%	−4.02%	−2.72%
	Lane 1	−8.27%	−2.74%	−1.82%	−3.99%	−2.28%	−2.07%	−2.68%	−1.92%	−1.86%	−2.43%
PCR	Lane 2	0.10%	−1.80%	−1.62%	−1.40%	−0.61%	0.43%	1.33%	1.24%	−2.21%	0.77%
	Lane 1	−1.99%	−3.02%	2.57%	−3.64%	2.35%	2.03%	1.69%	−1.24%	1.87%	−0.35%

Table 8. Relative Influence Ranking of the PCs as Predicting Variable of Adjacent Lanes PCs.

PC	Lane ID	DIR	SN	IRI	RUT	CI	TEXT	PSI	PCR	LAT	LON
IRI	Lane 2	1	2	4	5	10	6	7	9	3	8
	Lane 1	1	9	3	2	6	8	10	7	5	4
RUT	Lane 2	1	5	8	10	3	2	9	7	6	4
	Lane 1	1	10	9	2	6	3	8	4	5	7
CI	Lane 2	1	9	5	7	2	3	8	10	4	6
	Lane 1	1	5	3	2	8	6	9	4	7	10
TEXT	Lane 2	1	3	8	9	4	6	5	7	2	10
	Lane 1	1	7	9	8	2	3	10	6	4	5
PSI	Lane 2	1	4	7	10	2	9	5	8	3	6
	Lane 1	1	3	10	2	6	7	4	8	9	5
PCR	Lane 2	9	5	7	8	10	6	1	2	3	4
	Lane 1	6	2	3	1	4	5	8	9	7	10
Ave.	Lane 2	1	4	6	9	2	5	8	10	3	7
	Lane 1	1	8	7	2	4	3	10	6	5	9

3.4. S-MLR, Q-MLR, and ANN PCs Prediction Models

This section compiles the various model performance results for general comparison. The performance results for combined training and testing (All) for ANN models were selected to be paired with MLR models. Table 9 shows the summary of the RMSE values for all the PC indices prediction models. The trend is clear and consistent. ANN models showed lower RMSE than all the MLR models. Q-MLR models showed lower RMSE compared to the S-MLR model. The level of relative improvement in performance of the ANN model can only be fully understood by observing both the RMSE and the R^2 . Figure 9 shows the R^2 plot of the various PC indices prediction models. The ANN models showed better R^2 and are more general than all the MLR models. The gap in R^2 between ANN and S-MLR models range from 34% up to 68%, and from 19% to 36% relative to Q-MLR models.

Table 9. RMSE Summary of the Various S-MLR, Q-MLR, and ANN Models.

	IRI		RUT		CI		TEX		PSI		PCR	
	L 2	L 1	L 2	L 1	L 2	L 1	L 2	L 1	L 2	L 1	L 2	L 1
S-MLR	0.312	0.380	1.020	1.620	1.620	1.620	0.179	0.132	0.205	0.235	9.840	12.200
Q-MLR	0.251	0.323	0.883	1.430	1.180	1.190	0.136	0.104	0.163	0.200	7.880	11.000
ANN	0.216	0.281	0.708	1.133	0.797	0.874	0.093	0.084	0.143	0.167	9.277	9.992

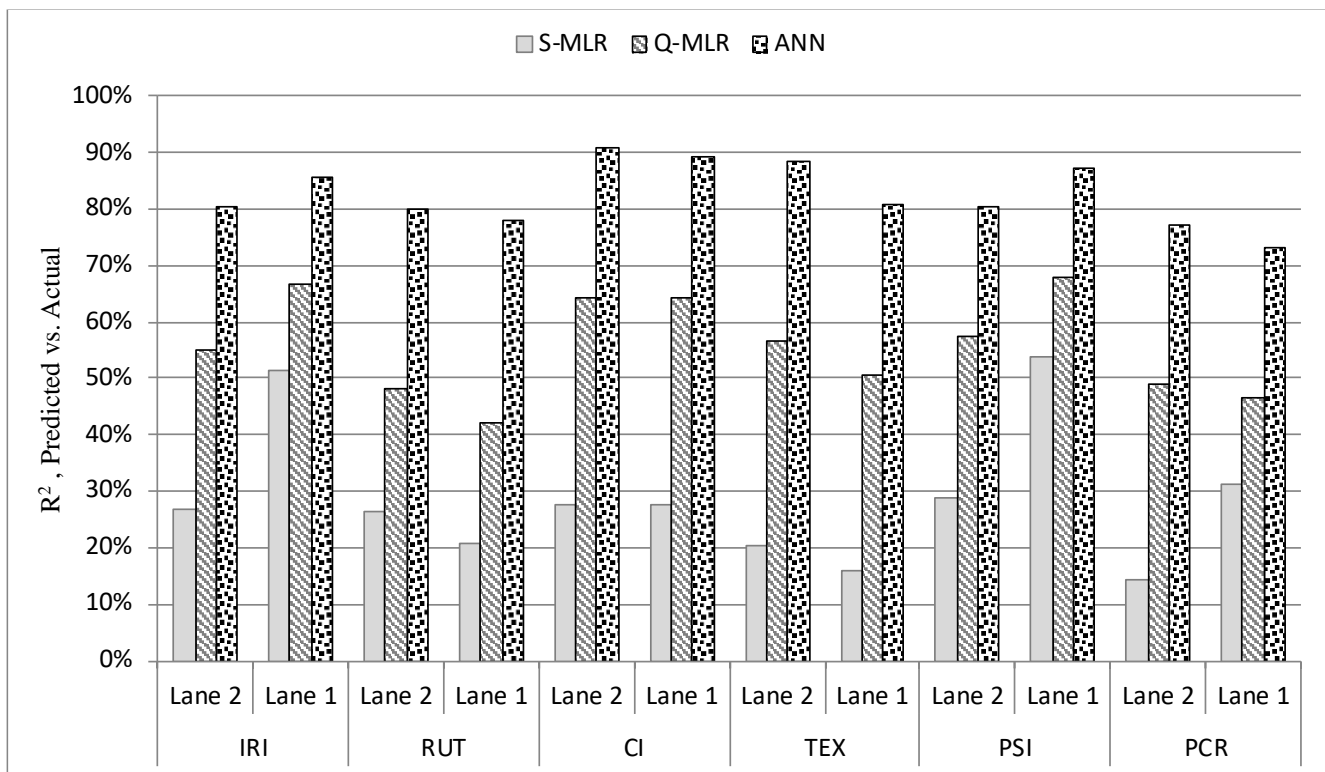


Figure 9. Comparison of MLR and ANN PC Predictive Model Performances In Terms of R^2 .

4. Conclusions and Recommendation

The feasibility of evaluating the pavement condition indices of a multi-lane highway by single lane inspection was examined. MLR and ANN were employed to model and predict the pavement distresses of multiple lanes as functions of pavement distresses of a single adjacent lane. Simple sensitivity analysis was conducted to assess the level of influence of the predicting PC variables on the ANN PC models. Below is the summary of key findings from this study:

- Although MLR models with interactive and higher order terms showed better performance than simple MLR models, MLR cannot be relied upon to adequately predict the PC indices of lanes as a function of adjacent lane PC variables.
- On the other hand, the ANN models showed promising performances that indicates the possibility of evaluating a multi-lane highway PC by single lane inspection. The gap in R^2 between ANN and S-MLR models ranges from 34% up to 68%, and from 19% to 36% relative to Q-MLR models.
- Traffic direction parameter, location and lane matching parameters contributed significantly to the performance of the ANN PC prediction models. This indicates the need for including other location dependent variables such as traffic volumes and pavement structural inputs.
- CI showed better predictability, followed by Tex, PSI, IRI, and RUT. The model PCR showed the least model performance. This suggests that other AI techniques other than ANN could be better suited for the lower-performing PCIs.
- Although an appreciable amount of data were utilized in this study, the outcomes of this study may not be valid for roads in other countries or even different cities. In addition, the study tested the models with PC data obtained from one class of road (free way) but from different locations. The results might not be valid for different class of roads.
- More similar studies using different AI techniques are recommended to make this approach common and practical.

Author Contributions: Conceptualization, M.A.D.; methodology, M.A.D., M.A. and A.J.; software, M.A.D. and F.A.; validation, S.A.O., F.A. and A.A.M.; formal analysis, S.A.O. and M.A.D.; investigation, A.J. and M.A.D.; resources, A.A.M.; data curation, A.J. and F.A.; writing—original draft preparation, M.A.D.; writing—review and editing, M.A., A.J. and M.A.D.; visualization, M.A.D., F.A. and S.A.O.; supervision, M.A.; project administration, F.A.; funding acquisition, M.A. All authors have read and agreed to the published version of the manuscript.

Funding: The APC of the article was funded by the Deanship of Scientific Research, Qassim University, Saudi Arabia.

Institutional Review Board Statement: Not applicable.

Informed Consent Statement: Not applicable.

Data Availability Statement: The data that support the findings of this study are available from the authors M.A.D. (madalhat@iau.edu.sa), upon reasonable request.

Acknowledgments: The researchers would like to thank the Deanship of Scientific Research, Qassim University for funding the publication of this project.

Conflicts of Interest: The authors declare no conflict of interest.

Appendix A

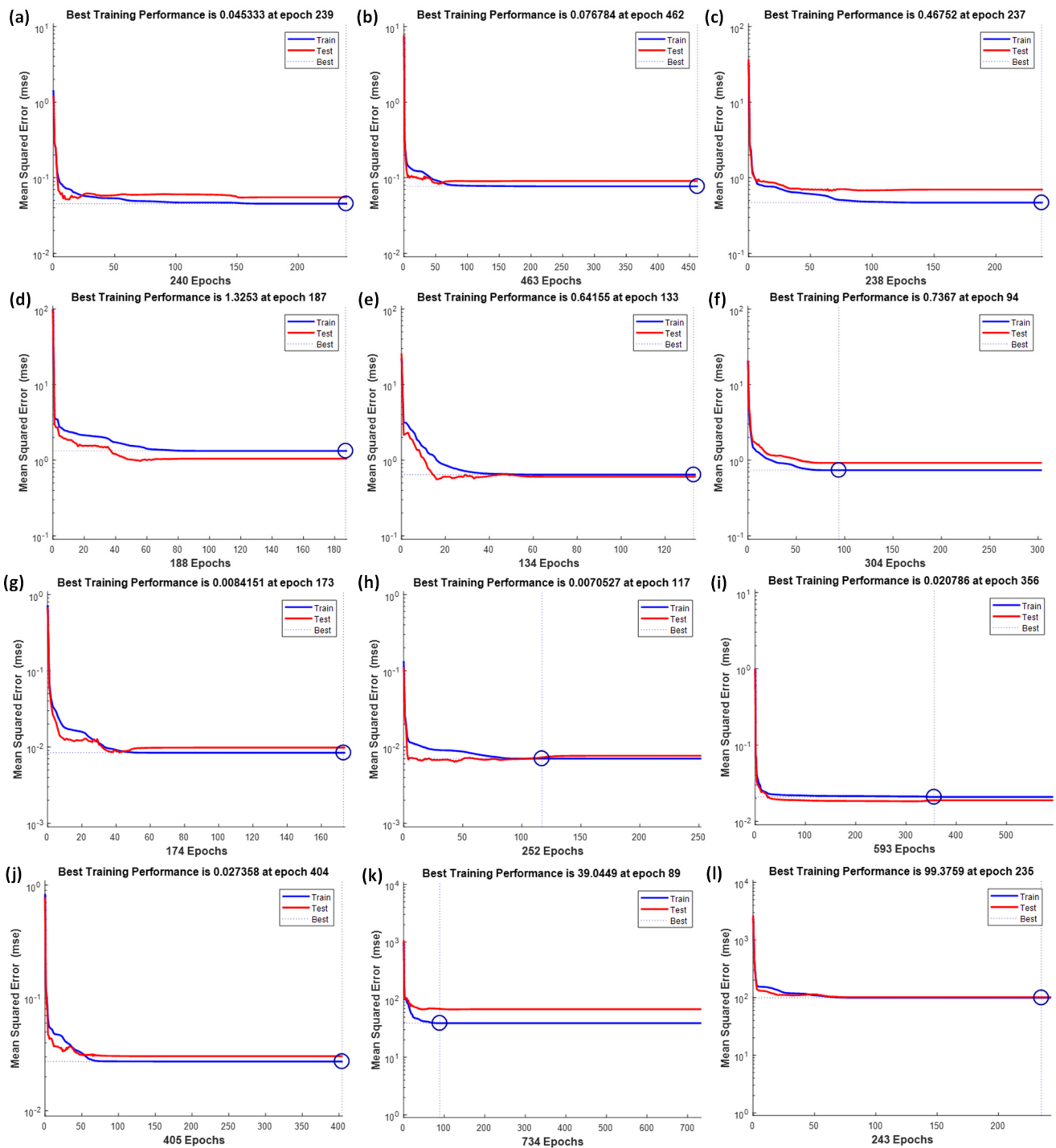


Figure A1. MSE vs Epochs for (a) IRI-L2, (b) IRI-L1, (c) RUT-L2, (d) RUT-L1, (e) CI-L2, (f) CI-L1, (g) Texture-L2, (h) Texture-L1, (i) PSI-L2, (j) PSI-L1, (k) PCR-L2, and (l) PCR-L1 ANN models.

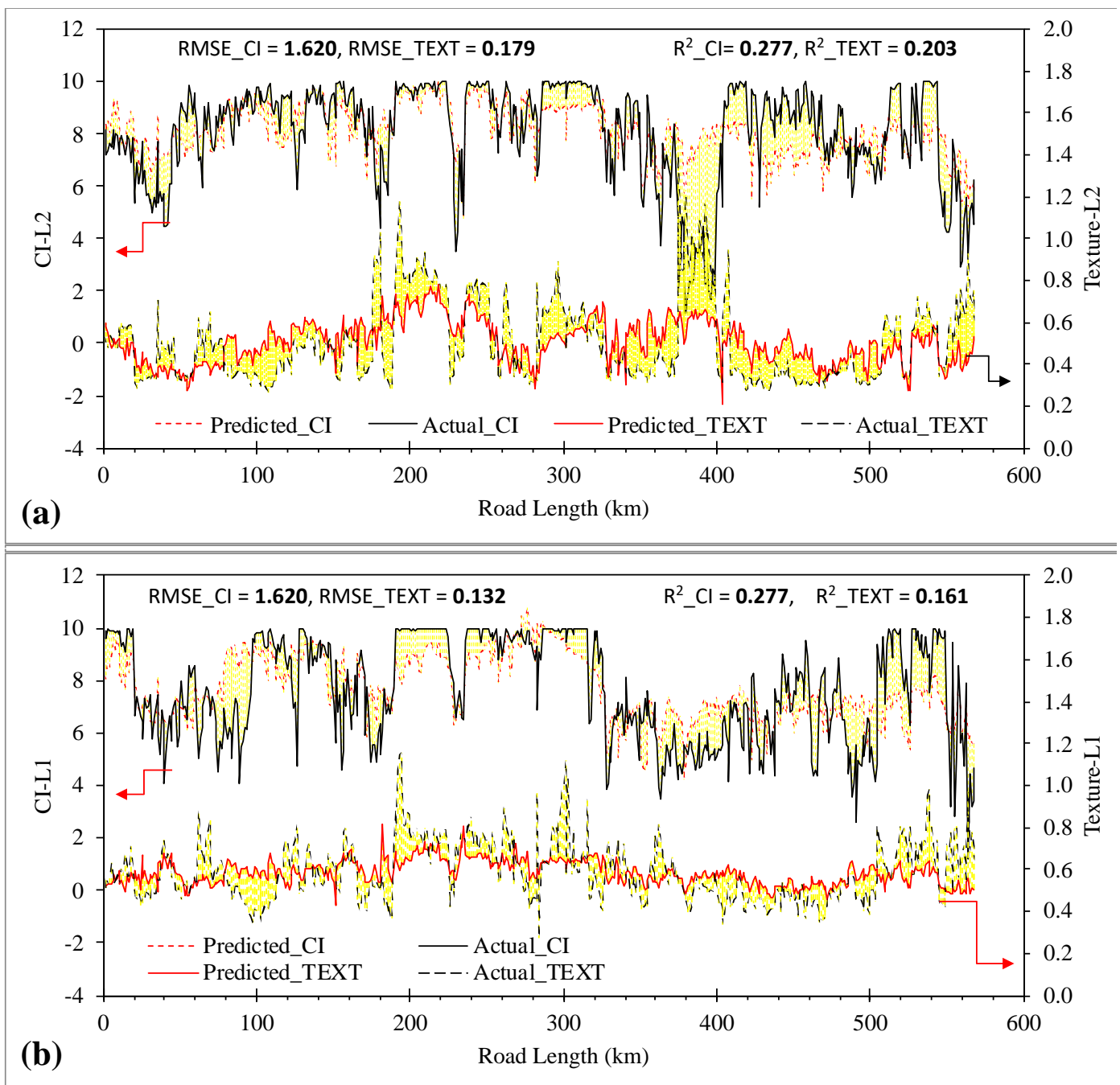


Figure A2. MLR Model, Predicted vs. Actual with Margin of Error for (a) Lane-2 CI and Texture, and (b) Lane-1 CI and Texture.

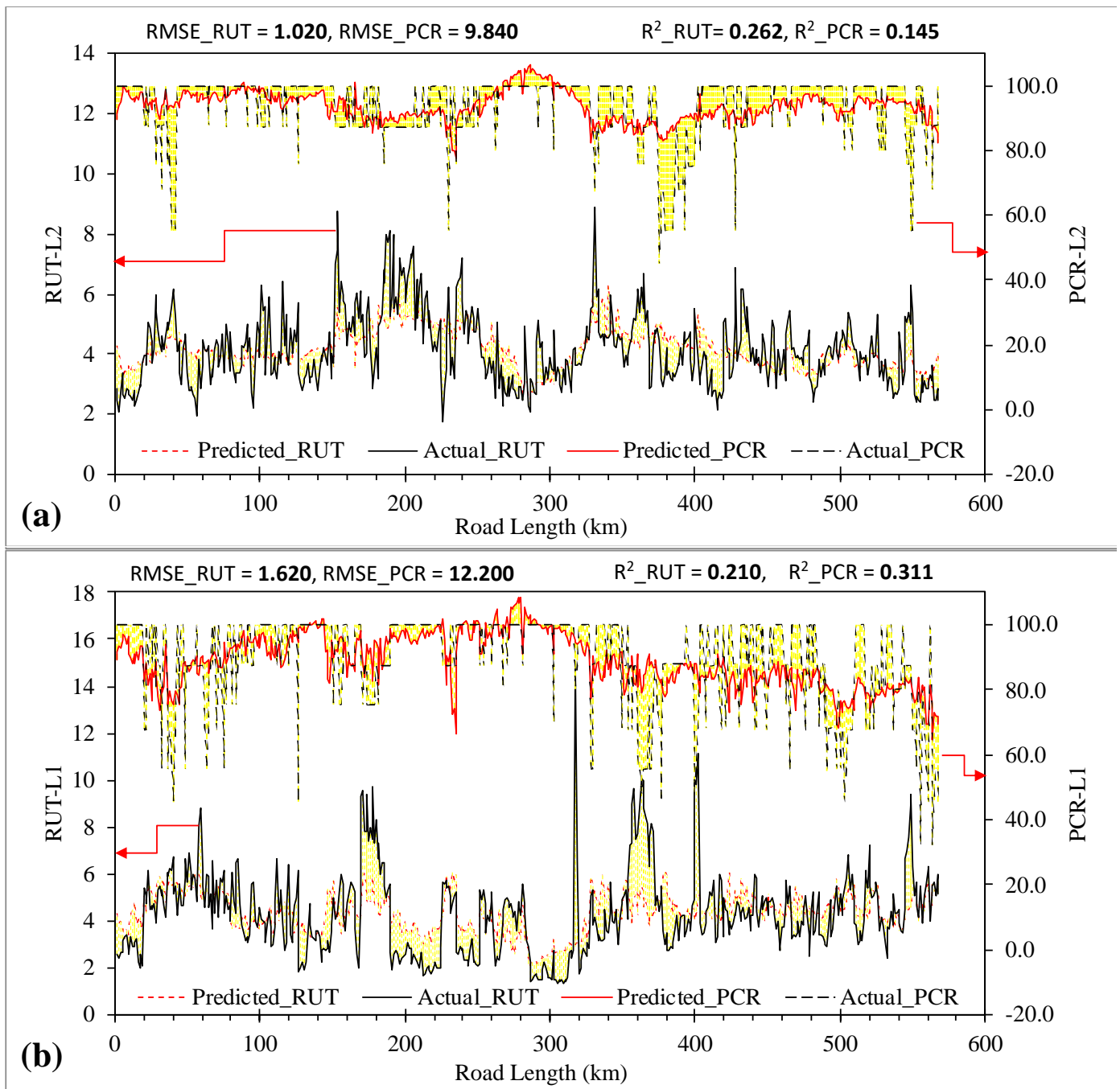


Figure A3. MLR Model, Predicted vs. Actual with Margin of Error for (a) Lane-2 RUT and PCR, and (b) Lane-1 RUT and PCR.

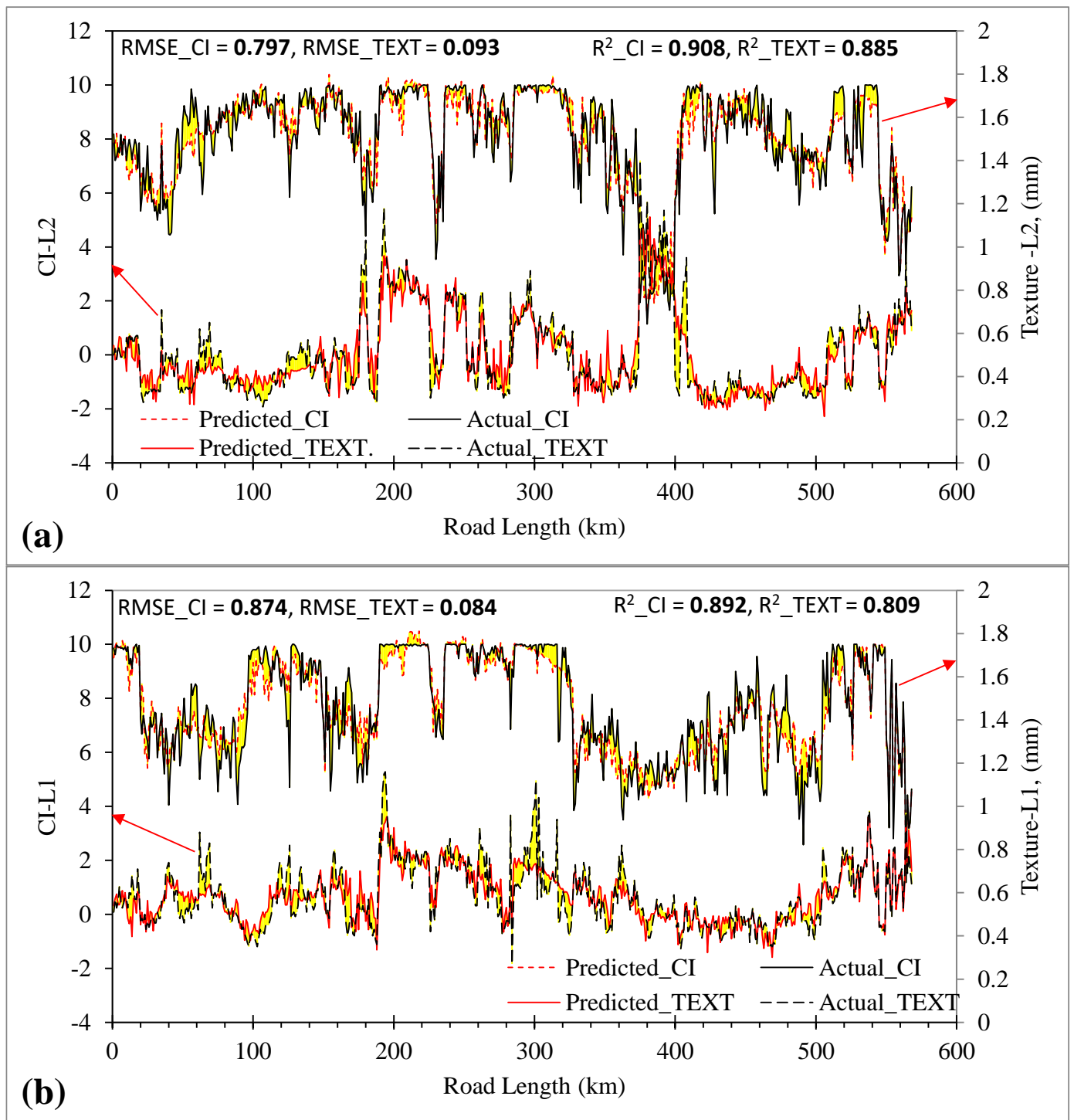


Figure A4. ANN Model, Predicted vs. Actual with Margin of Error for (a) Lane-2 CI and Texture, and (b) Lane-1 CI and Texture.

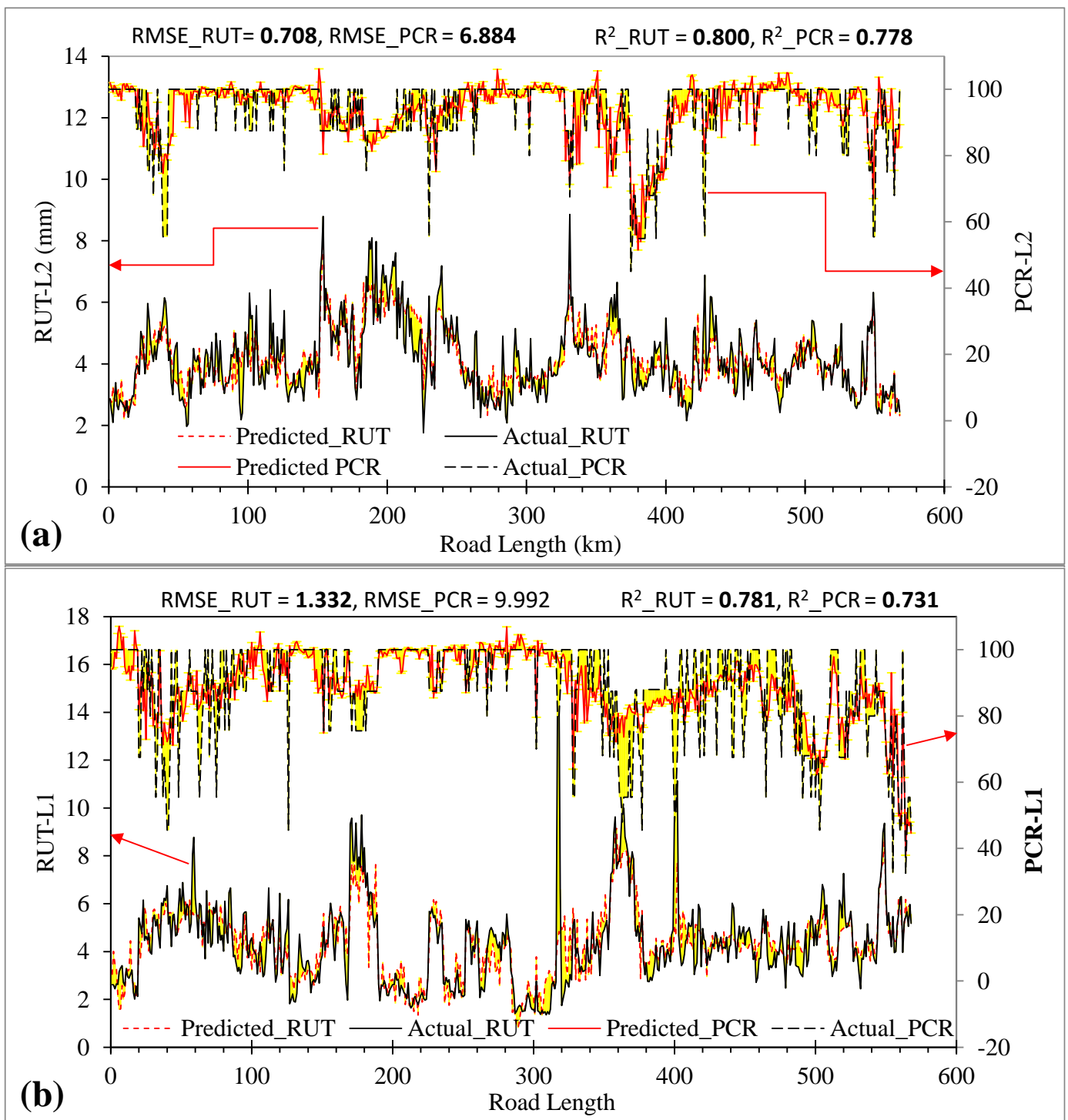


Figure A5. ANN Model, Predicted vs. Actual with Margin of Error for (a) Lane-2 RUT and PCR, and (b) Lane-1 RUT and PCR.

Table A1. Summary of Average RMSE and R² for the ANN PC Models after Variables Exclusion.

RMSE											
PC	Lane ID	Without DIR	Without SN	Without IRI	Without RUT	Without CI	Without TEXT	Without PSI	Without PCR	Without LAT	Without LON
IRI	Lane 2	0.2487	0.2377	0.2352	0.2336	0.2285	0.2336	0.2328	0.2290	0.2375	0.2325
	Lane 1	0.3100	0.2973	0.3022	0.3030	0.2991	0.2980	0.2971	0.2982	0.3020	0.3021
RUT	Lane 2	0.8642	0.7807	0.7758	0.7618	0.8030	0.8051	0.7678	0.7757	0.7800	0.7866
	Lane 1	1.3015	1.1574	1.1687	1.2287	1.2345	1.2177	1.1734	1.2503	1.2155	1.2097
CI	Lane 2	1.0021	0.8332	0.8623	0.8509	0.9060	0.8705	0.8458	0.8163	0.8640	0.8613
	Lane 1	1.0744	0.9369	0.9540	0.9545	0.9257	0.9363	0.9029	0.9512	0.9359	0.9024
TEXT	Lane 2	0.1108	0.1008	0.0953	0.0953	0.0994	0.0969	0.0982	0.0964	0.1010	0.0944
	Lane 1	0.1007	0.0896	0.0891	0.0895	0.0937	0.0935	0.0883	0.0897	0.0916	0.0899
PSI	Lane 2	0.1568	0.1522	0.1511	0.1481	0.1547	0.1497	0.1517	0.1511	0.1545	0.1512
	Lane 1	0.2072	0.1823	0.1778	0.1883	0.1800	0.1790	0.1821	0.1785	0.1780	0.1806
PCR	Lane 2	6.7656	6.9566	6.9350	6.9375	6.8403	6.7263	6.6500	6.6592	7.0250	6.7175
	Lane 1	10.2974	10.4041	9.7632	10.4608	9.7885	9.8416	9.8722	10.2101	9.8633	10.1149
R ²											
PC	Lane ID	Without DIR	Without SN	Without IRI	Without RUT	Without CI	Without TEXT	Without PSI	Without PCR	Without LAT	Without LON
IRI	Lane 2	73.38%	75.99%	76.53%	76.85%	78.07%	76.91%	77.05%	77.95%	75.94%	77.23%
	Lane 1	82.32%	83.93%	83.27%	83.17%	83.77%	83.79%	83.91%	83.79%	83.32%	83.30%
RUT	Lane 2	68.62%	75.55%	75.94%	76.86%	73.91%	73.74%	76.50%	75.91%	75.68%	75.16%
	Lane 1	70.20%	76.21%	76.10%	73.17%	74.82%	73.85%	76.00%	74.41%	74.81%	75.87%
CI	Lane 2	85.25%	90.06%	89.35%	89.61%	88.16%	89.10%	89.74%	90.48%	89.29%	89.32%
	Lane 1	83.38%	87.61%	87.13%	87.15%	87.97%	87.66%	88.57%	87.19%	87.68%	88.62%
TEXT	Lane 2	83.46%	86.53%	88.11%	88.12%	86.94%	87.70%	87.23%	87.77%	86.61%	88.32%
	Lane 1	71.67%	78.45%	78.72%	78.48%	76.11%	76.20%	79.09%	78.34%	77.30%	78.23%
PSI	Lane 2	76.42%	77.98%	78.33%	79.30%	77.14%	78.90%	78.14%	78.41%	77.24%	78.29%
	Lane 1	80.20%	85.03%	85.84%	83.94%	85.44%	85.62%	85.08%	85.75%	85.80%	85.31%
PCR	Lane 2	77.42%	75.95%	76.09%	76.26%	76.87%	77.68%	78.37%	78.30%	75.63%	77.94%
	Lane 1	71.63%	70.88%	74.97%	70.42%	74.80%	74.57%	74.32%	72.18%	74.45%	72.83%

References

- Sadek, A.W. Artificial Intelligence Applications in Transportation. In *Transportation Research Circular*; Transportation Research Board, Artificial Intelligence and Advanced Computing Applications Committee: Washington, DC, USA, 2007; pp. 1–7.
- Qi, Y.; Zhang, S.; Jiang, F.; Zhou, H.; Tao, D.; Li, X. Siamese Local and Global Networks for Robust Face Tracking. *IEEE Trans. Image Process.* **2020**, *29*, 9152–9164. [[CrossRef](#)] [[PubMed](#)]
- Yang, Y.; Li, G.; Qi, Y.; Huang, Q. Release the Power of Online-Training for Robust Visual Tracking. *Proc. AAAI Conf. Artif. Intell.* **2020**, *34*, 12645–12652. [[CrossRef](#)]
- Qi, Y.; Qin, L.; Zhang, S.; Huang, Q.; Yao, H. Robust Visual Tracking via Scale-and-State-Awareness. *Neurocomputing* **2019**, *329*, 75–85. [[CrossRef](#)]
- An, D.; Qi, Y.; Huang, Y.; Wu, Q.; Wang, L.; Tan, T. Neighbor-View Enhanced Model for Vision and Language Navigation. In Proceedings of the 29th ACM International Conference on Multimedia, Virtual, 20–24 October 2021; pp. 5101–5109.
- Zhu, W.; Qi, Y.; Narayana, P.; Sone, K.; Basu, S.; Wang, X.E.; Wu, Q.; Eckstein, M.; Wang, W.Y. Diagnosing Vision-and-Language Navigation: What Really Matters. *arXiv* **2021**, arXiv:2103.16561.
- Qi, Y.; Pan, Z.; Hong, Y.; Yang, M.-H.; van den Hengel, A.; Wu, Q. The Road to Know-Where: An Object-and-Room Informed Sequential Bert for Indoor Vision-Language Navigation. In Proceedings of the IEEE/CVF International Conference on Computer Vision, Virtual, 11–17 October 2021; pp. 1655–1664.
- Wang, Y.; Qi, Y.; Yao, H.; Gong, D.; Wu, Q. Image Editing with Varying Intensities of Processing. *Comput. Vis. Image Underst.* **2021**, *211*, 103260. [[CrossRef](#)]
- Ye, H.; Li, G.; Qi, Y.; Wang, S.; Huang, Q.; Yang, M.-H. Hierarchical Modular Network for Video Captioning. In Proceedings of the IEEE/CVF Conference on Computer Vision and Pattern Recognition, New Orleans, LA, USA, 19–24 June 2022; pp. 17939–17948.

10. Chen, W.; Hong, D.; Qi, Y.; Han, Z.; Wang, S.; Qing, L.; Huang, Q.; Li, G. Multi-Attention Network for Compressed Video Referring Object Segmentation. In Proceedings of the 30th ACM International Conference on Multimedia, Lisbon, Portugal, 10–14 October 2022; pp. 4416–4425.
11. Sattar, K.; Chikh Oughali, F.; Assi, K.; Ratrou, N.; Jamal, A.; Masiur Rahman, S. Transparent Deep Machine Learning Framework for Predicting Traffic Crash Severity. *Neural Comput. Appl.* **2022**, 1–13. [\[CrossRef\]](#)
12. Moslem, S.; Farooq, D.; Jamal, A.; Almarhabi, Y.; Almoshaogeh, M.; Butt, F.M.; Tufail, R.F. An Integrated Fuzzy Analytic Hierarchy Process (AHP) Model for Studying Significant Factors Associated with Frequent Lane Changing. *Entropy* **2022**, *24*, 367. [\[CrossRef\]](#)
13. Jamal, A.; Zahid, M.; Tauhidur Rahman, M.; Al-Ahmadi, H.M.; Almoshaogeh, M.; Farooq, D.; Ahmad, M. Injury Severity Prediction of Traffic Crashes with Ensemble Machine Learning Techniques: A Comparative Study. *Int. J. Inj. Control. Saf. Promot.* **2021**, *28*, 408–427. [\[CrossRef\]](#)
14. Ijaz, M.; Lan, L.; Zahid, M.; Jamal, A. A Comparative Study of Machine Learning Classifiers for Injury Severity Prediction of Crashes Involving Three-Wheeled Motorized Rickshaw. *Accid. Anal. Prev.* **2021**, *154*, 106094. [\[CrossRef\]](#)
15. Tamim Kashifi, M.; Jamal, A.; Samim Kashfi, M.; Almoshaogeh, M.; Masiur Rahman, S. Predicting the Travel Mode Choice with Interpretable Machine Learning Techniques: A Comparative Study. *Travel Behav. Soc.* **2022**, *29*, 279–296. [\[CrossRef\]](#)
16. Ullah, I.; Liu, K.; Yamamoto, T.; Shafiullah, M.; Jamal, A. Grey Wolf Optimizer-Based Machine Learning Algorithm to Predict Electric Vehicle Charging Duration Time. *Transp. Lett.* **2022**, 1–18. [\[CrossRef\]](#)
17. Ullah, I.; Liu, K.; Yamamoto, T.; Al Mamlook, R.E.; Jamal, A. A Comparative Performance of Machine Learning Algorithm to Predict Electric Vehicles Energy Consumption: A Path towards Sustainability. *Energy Environ.* **2021**, *33*, 1583–1612. [\[CrossRef\]](#)
18. Ullah, I.; Liu, K.; Yamamoto, T.; Zahid, M.; Jamal, A. Prediction of Electric Vehicle Charging Duration Time Using Ensemble Machine Learning Algorithm and Shapley Additive Explanations. *Int. J. Energy Res.* **2022**, *46*, 15211–15230. [\[CrossRef\]](#)
19. Alkhulaifi, A.; Jamal, A.; Ahmad, I. Predicting Traffic Sign Retro-Reflectivity Degradation Using Deep Neural Networks. *Appl. Sci.* **2021**, *11*, 11595. [\[CrossRef\]](#)
20. Jamal, A.; Reza, I.; Shafiullah, M. Modeling Retroreflectivity Degradation of Traffic Signs Using Artificial Neural Networks. *IATSS Res.* **2022**, *46*. [\[CrossRef\]](#)
21. Sundin, S.; Braban-Ledoux, C. Artificial Intelligence–Based Decision Support Technologies in Pavement Management. *Comput.-Aided Civ. Infrastruct. Eng.* **2001**, *16*, 143–157. [\[CrossRef\]](#)
22. Ceylan, H.; Bayrak, M.B.; Gopalakrishnan, K. Neural Networks Applications in Pavement Engineering: A Recent Survey. *Int. J. Pavement Res. Technol.* **2014**, *7*, 434–444.
23. Flintsch, G.W.; Chen, C. Soft Computing Applications in Infrastructure Management. *J. Infrastruct. Syst.* **2004**, *10*, 157–166. [\[CrossRef\]](#)
24. Shahnazari, H.; Tutunchian, M.A.; Mashayekhi, M.; Amini, A.A. Application of Soft Computing for Prediction of Pavement Condition Index. *J. Transp. Eng.* **2012**, *138*, 1495–1506. [\[CrossRef\]](#)
25. Umer, A.; Hewage, K.; Haider, H.; Sadiq, R. Sustainability Evaluation Framework for Pavement Technologies: An Integrated Life Cycle Economic and Environmental Trade-off Analysis. *Transp. Res. Part D Transp. Environ.* **2017**, *53*, 88–101. [\[CrossRef\]](#)
26. Gopalakrishnan, K. Instantaneous Pavement Condition Evaluation Using Non-Destructive Neuro-Evolutionary Approach. *Struct. Infrastruct. Eng.* **2012**, *8*, 857–872. [\[CrossRef\]](#)
27. Koduru, H.K.; Xiao, F.; Amirhanian, S.N.; Juang, C.H. Using Fuzzy Logic and Expert System Approaches in Evaluating Flexible Pavement Distress: Case Study. *J. Transp. Eng.* **2010**, *136*, 149–157. [\[CrossRef\]](#)
28. Bosurgi, G.; Trifirò, F. A Model Based on Artificial Neural Networks and Genetic Algorithms for Pavement Maintenance Management. *Int. J. Pavement Eng.* **2005**, *6*, 201–209. [\[CrossRef\]](#)
29. Zhou, G.; Wang, L.; Wang, D.; Reichle, S. Integration of GIS and Data Mining Technology to Enhance the Pavement Management Decision Making. *J. Transp. Eng.* **2010**, *136*, 332–341. [\[CrossRef\]](#)
30. Mubarak, M. Highway Subsurface Assessment Using Pavement Surface Distress and Roughness Data. *Int. J. Pavement Res. Technol.* **2016**, *9*, 393–402. [\[CrossRef\]](#)
31. Ziari, H.; Sobhani, J.; Ayoubinejad, J.; Hartmann, T. Prediction of IRI in Short and Long Terms for Flexible Pavements: ANN and GMDH Methods. *Int. J. Pavement Eng.* **2016**, *17*, 776–788. [\[CrossRef\]](#)
32. Elhadidy, A.A.; El-Badawy, S.M.; Elbeltagi, E.E. A Simplified Pavement Condition Index Regression Model for Pavement Evaluation. *Int. J. Pavement Eng.* **2021**, *22*, 643–652. [\[CrossRef\]](#)
33. Bianchini, A.; Bandini, P. Prediction of Pavement Performance through Neuro-Fuzzy Reasoning. *Comput.-Aided Civ. Infrastruct. Eng.* **2010**, *25*, 39–54. [\[CrossRef\]](#)
34. Luo, C. Pavement Deterioration Modeling and Design of a Composite Pavement Distress Index for Kentucky Interstate Highways and Parkways. Master's Thesis, University of Louisville, Louisville, KY, USA, 2014.
35. Zhang, W.; Durango-Cohen, P.L. Explaining Heterogeneity in Pavement Deterioration: Clusterwise Linear Regression Model. *J. Infrastruct. Syst.* **2014**, *20*, 04014005. [\[CrossRef\]](#)
36. Swei, O.; Gregory, J.; Kirchain, R. Does Pavement Degradation Follow a Random Walk with Drift? Evidence from Variance Ratio Tests for Pavement Roughness. *J. Infrastruct. Syst.* **2018**, *24*, 04018027. [\[CrossRef\]](#)
37. Attoh-Okine, N.O. Grouping Pavement Condition Variables for Performance Modeling Using Self-Organizing Maps. *Comput.-Aided Civ. Infrastruct. Eng.* **2001**, *16*, 112–125. [\[CrossRef\]](#)

38. Tabatabaee, N.; Ziyadi, M.; Shafahi, Y. Two-Stage Support Vector Classifier and Recurrent Neural Network Predictor for Pavement Performance Modeling. *J. Infrastruct. Syst.* **2013**, *19*, 266–274. [CrossRef]
39. Barzegaran, J.; Shahni Dezfoulian, R.; Fakhri, M. Estimation of IRI from PASER Using ANN Based on K-Means and Fuzzy c-Means Clustering Techniques: A Case Study. *Int. J. Pavement Eng.* **2021**, 1–15. [CrossRef]
40. Majidifard, H.; Adu-Gyamfi, Y.; Buttlar, W.G. Deep Machine Learning Approach to Develop a New Asphalt Pavement Condition Index. *Constr. Build. Mater.* **2020**, *247*, 118513. [CrossRef]
41. Roberts, R.; Giancontieri, G.; Inzerillo, L.; Di Mino, G. Towards Low-Cost Pavement Condition Health Monitoring and Analysis Using Deep Learning. *Appl. Sci.* **2020**, *10*, 319. [CrossRef]
42. Chen, C.; Chandra, S.; Han, Y.; Seo, H. Deep Learning-Based Thermal Image Analysis for Pavement Defect Detection and Classification Considering Complex Pavement Conditions. *Remote Sens.* **2021**, *14*, 106. [CrossRef]
43. Marcelino, P.; de Lurdes Antunes, M.; Fortunato, E.; Gomes, M.C. Machine Learning Approach for Pavement Performance Prediction. *Int. J. Pavement Eng.* **2021**, *22*, 341–354. [CrossRef]
44. Inkoom, S.; Sobanjo, J.; Barbu, A.; Niu, X. Prediction of the Crack Condition of Highway Pavements Using Machine Learning Models. *Struct. Infrastruct. Eng.* **2019**, *15*, 940–953. [CrossRef]
45. Sholevar, N.; Golroo, A.; Esfahani, S.R. Machine Learning Techniques for Pavement Condition Evaluation. *Autom. Constr.* **2022**, *136*, 104190. [CrossRef]
46. Wang, K.C. Designs and Implementations of Automated Systems for Pavement Surface Distress Survey. *J. Infrastruct. Syst.* **2000**, *6*, 24–32. [CrossRef]
47. Özdemir, O.B.; Soydan, H.; Yardımcı Çetin, Y.; Düzgün, H.Ş. Neural Network Based Pavement Condition Assessment with Hyperspectral Images. *Remote Sens.* **2020**, *12*, 3931. [CrossRef]
48. Chambon, S.; Moliard, J.-M. Automatic Road Pavement Assessment with Image Processing: Review and Comparison. *Int. J. Geophys.* **2011**, *2011*, 1–20. [CrossRef]
49. Ritchie, S.G.; Kaseko, M.; Bavarian, B. *Development of an Intelligent System for Automated Pavement Evaluation*; Transportation Research Board: Washington, DC, USA, 1991.
50. Wang, K.C.; Li, Q.J.; Yang, G.; Zhan, Y.; Qiu, Y. Network Level Pavement Evaluation with 1 Mm 3D Survey System. *J. Traffic Transp. Eng. Engl. Ed.* **2015**, *2*, 391–398. [CrossRef]
51. Coenen, T.B.; Golroo, A. A Review on Automated Pavement Distress Detection Methods. *Cogent Eng.* **2017**, *4*, 1374822. [CrossRef]
52. Arhin, S.A.; Noel, E.C.; Ribbiso, A. Acceptable International Roughness Index Thresholds Based on Present Serviceability Rating. *J. Civ. Eng. Res.* **2015**, *5*, 90–96.
53. Bardeesi, M.W.; Attallah, Y. Evaluation of Pavement Conditions and Maintenance Works for Road Network in Saudi Arabia. *Eur. Sci. J.* **2015**, *11*, 261–278.
54. Miller, J.S.; Bellinger, W.Y. *Distress Identification Manual for the Long-Term Pavement Performance Program*; United States Federal Highway Administration, Office of Infrastructure: Washington, DC, USA, 2003.
55. Cary, W.N. The Pavement Serviceability-Performance Concept. Highway Research Board Bulletin. 1960, p. 250. Available online: <https://onlinepubs.trb.org/Onlinepubs/hrbulletin/250/250-003.pdf> (accessed on 28 November 2022).
56. Welch, B.L. On the Comparison of Several Mean Values: An Alternative Approach. *Biometrika* **1951**, *38*, 330–336. [CrossRef]
57. Abiodun, O.I.; Jantan, A.; Omolara, A.E.; Dada, K.V.; Mohamed, N.A.; Arshad, H. State-of-the-Art in Artificial Neural Network Applications: A Survey. *Heliyon* **2018**, *4*, e00938. [CrossRef]
58. Jamal, A.; Umer, W. Exploring the Injury Severity Risk Factors in Fatal Crashes with Neural Network. *Int. J. Environ. Res. Public Health* **2020**, *17*, 7466. [CrossRef]
59. MacKay, D.J. Bayesian Interpolation. *Neural Comput.* **1992**, *4*, 415–447. [CrossRef]
60. Foresee, F.D.; Hagan, M.T. Gauss-Newton Approximation to Bayesian Learning. In Proceedings of the International Conference on Neural Networks (ICNN'97), Houston, TX, USA, 12 June 1997; IEEE: Piscataway, NJ, USA, 1997; Volume 3, pp. 1930–1935.
61. Burden, F.; Winkler, D. Bayesian Regularization of Neural Networks. *Artif. Neural Netw.* **2008**, *458*, 23–42.
62. Ruben, G.B.; Zhang, K.; Bao, H.; Ma, X. Application and Sensitivity Analysis of Artificial Neural Network for Prediction of Chemical Oxygen Demand. *Water Resour. Manag.* **2018**, *32*, 273–283. [CrossRef]

Disclaimer/Publisher's Note: The statements, opinions and data contained in all publications are solely those of the individual author(s) and contributor(s) and not of MDPI and/or the editor(s). MDPI and/or the editor(s) disclaim responsibility for any injury to people or property resulting from any ideas, methods, instructions or products referred to in the content.